Titre: Title:	A Pseudo-3D Ball Lattice Artifact and Method for Evaluating the Metrological Performance of Structured-Light 3D Scanners
Auteur: Author:	Pooya Ghandali
Date:	2018
Type:	Mémoire ou thèse / Dissertation or Thesis
Référence: Citation:	Ghandali, P. (2018). A Pseudo-3D Ball Lattice Artifact and Method for Evaluating the Metrological Performance of Structured-Light 3D Scanners [Mémoire de maîtrise, École Polytechnique de Montréal]. PolyPublie. https://publications.polymtl.ca/3773/

URL de PolyPublie: PolyPublie URL:	https://publications.polymtl.ca/3773/
Directeurs de recherche: Advisors:	Farbod Khameneifar, & J. R. René Mayer
Programme: Program:	Génie mécanique

UNIVERSITÉ DE MONTRÉAL

A PSEUDO-3D BALL LATTICE ARTIFACT AND METHOD FOR EVALUATING THE METROLOGICAL PERFORMANCE OF STRUCTURED-LIGHT 3D SCANNERS

POOYA GHANDALI

DÉPARTEMENT DE GÉNIE MÉCANIQUE

ÉCOLE POLYTECHNIQUE DE MONTRÉAL

MÉMOIRE PRÉSENTÉ EN VUE DE L'OBTENTION

DU DIPLÔME DE MAÎTRISE ÈS SCIENCES APPLIQUÉES

(GÉNIE MÉCANIQUE)

DÉCEMBRE 2018

UNIVERSITÉ DE MONTRÉAL

ÉCOLE POLYTECHNIQUE DE MONTRÉAL

Ce mémoire intitulé :

A PSEUDO-3D BALL LATTICE ARTIFACT AND METHOD FOR EVALUATING THE METROLOGICAL PERFORMANCE OF STRUCTURED-LIGHT 3D SCANNERS

présenté par : GHANDALI Pooya

en vue de l'obtention du diplôme de : Maîtrise és sciences appliquées

a été dûment accepté par le jury d'examen constitué de :

M. BALAZINSKI Marek, Docteur és sciences, président

M. KHAMENEIFAR Farbod, Ph. D., membre et directeur de recherche

M. MAYER René, Ph. D., membre et codirecteur de recherche

M. BARON Luc, Ph. D., membre

DEDICATION

To my family.

ACKNOWLEDGEMENTS

Firstly, I would like to thank my principle supervisor Prof. Farbod Khameneifar, and my co-supervisor Prof. Rene Mayer who have helped and supported me during this research.

Next, Mr. Guy Gironne, the technician in Virtual Manufacturing Laboratory (LRFV) of Polytechnique Montreal for his help in the artifact's fabrication and measurement.

Thanks to my lab mates for their supports and advises during this research.

Thanks to Fereshteh Nikfarjam for her help during my studies.

And finally, but the most important appreciation to my family, my parents and my brother, for their true supports and encourages during each step of my life.

RÉSUMÉ

Malgré la croissance de la popularité des scanners 3D et le besoin de leurs utilisateurs d'évaluer leur performance métrologique, Il n'existe aucune norme internationale d'évaluation de leur performance métrologique. Les utilisateurs de ces scanners ont besoin des tests d'acceptations afin de vérifier l'éligibilité d'un scanner pour une mesure spécifique, ainsi que des paramètres quantifiés pour comparer différents scanners 3D à lumière structurée. Ce projet a pour but de proposer une méthode systématique d'évaluation de la performance métrologique des scanners 3D à lumière structurée. Puisque les scanners 3D à lumière structurée, aussi appelés systèmes de projection franges, sont des dispositifs de numérisation d'aire, leur performance doit être évaluée dans tout leur volume de mesure. Dans ce travail, un artefact pseudo-3D, composé d'une plaque à billes 2D et trois composants d'espacement, est proposé avec une nouvelle procédure d'analyse des données pour l'évaluation des données du scanner selon des valeurs de référence de l'artefact. Dans la procédure d'évaluation de performance développée, les erreurs de la mesure de la taille, de la forme et des distances différentes sont étudiées. Les données de référence des distances sont fournies en mesurant l'artefact par une machine à mesurer tridimensionnelle (MMT) avant d'être mesuré par un scanner 3D. L'incertitude standard des valeurs de référence des distances sont estimées, ce qui correspond à 1,45 µm. Les billes de précision fournissent les données de référence pour la taille et la forme. L'incertitude standard du diamètre et la forme (sphéricité) des billes est indiquée par leur fournisseur (Bal-tec) à $0.64\,\mu m$. La méthode proposée offre à ses utilisateurs des tests d'acceptations, ainsi qu'un aperçu complet de la performance du scanner 3D à lumières structurée pour mesurer la distance, la taille et la forme à différentes positions dans son volume de numérisation.

ABSTRACT

Despite the increasing popularity of structured-light 3D scanners, there exists no international standard for assessing their metrological performance. The users of these scanners need acceptance tests to verify the eligibility of a scanner for specific measurements, as well as quantified metrics to compare different structured-light 3D scanners. This project aims to propose a systematic method for evaluating the metrological performance of the structured light scanners. Since the structured-light 3D scanners, also known as fringe projection systems, are area-scanning devices, they require their performance to be evaluated in their measurement volume. In this work, a pseudo-3D artifact, consisting of a 2D ball-plate and three spacers, is proposed along with a novel data analysis procedure for benchmarking the scanner's data based on the reference values of the artifact. In the developed performance evaluation procedure, errors in measuring distance, size, and form are investigated. The reference data in investigating various distances is provided by measuring the artifact by a coordinate measuring machine (CMM) before its measurement by a 3D scanner. The uncertainty of the reference values of the distances is estimated, which is $1.45\ \mu m$. The precision balls provide the reference of the size and form. The uncertainty of the diameter and the form (sphericity) of the balls is reported by their supplier (Bal-tec) as $0.64\ \mu m$. The proposed method provides its users with acceptance tests, as well as a comprehensive insight into the performance of the structured light 3D scanner in measuring distance, size, and form at different positions within its entire scanning volume.

TABLE OF CONTENTS

DEDICATION III

ACKNOWLEDGEMENTS IV

RÉSUMÉ V

ABSTRACT VI

TABLE OF CONTENTS VII

LIST OF TABLES IX

LIST OF FIGURES X

LIST OF SYMBOLS AND ABBREVIATIONS XI

LIST OF APPENDICES XII

CHAPTER 1 INTRODUCTION 1

1.1 General introduction 1

1.2 Problem definition 3

1.3 Research objective 3

1.4 Thesis outline 3

CHAPTER 2 LITERATURE REVIEW 4

CHAPTER 3 METHODOLOGY 9

3.1 Artifact design and fabrication 9

3.2 Artifact measurement 9

3.3 3D scanner's performance evaluation procedure 9

CHAPTER 4 ARTICLE 1: A PSEUDO-3D BALL LATTICE ARTIFACT AND METHOD FOR EVALUATING THE METROLOGICAL PERFORMANCE OF STRUCTURED-LIGHT 3D SCANNERS 11

4.1 Abstract 11

4.2 Introduction 12

4.3 Designed reference artifact 15
4.4 Proposed performance evaluation procedure 19
4.4.1 Artifact measurement 19
4.4.2 Investigated parameters 21
4.4.2.1 Error in distance measurement 22
4.4.2.2 Error in size and form measurement 23
4.4.3 Uncertainty of the reference data 26
4.5 Conclusions 28
4.6 Acknowledgments 29
4.7 References 29
CHAPTER 5 GENERAL DISCUSSION 32
CHAPTER 6 CONCLUSION AND RECOMMENDATIONS 35
BIBLIOGRAPHY 36
APPENDICES 39

LIST OF TABLES

Table 4.1: Error in size measurement for each level and the 3D grid (units in mm). 26

Table 4.2: Error in form measurement for each level and the 3D grid (units in mm). 26

Table 4.3: The uncertainty of the reference data for the investigated parameters. 28

Table 5.1. Maximum error, mean of the absolute errors, and standard deviation of the errors in measuring each parameter 34

LIST OF FIGURES

Figure 1.1: Laser scanner's scanning plane 1

Figure 1.2: The concept of the scanning volume in structured light scanning..... 2

Figure 2.1: The used artifact to follow VDI/VDE 2634 part 2 by Erickson et al. [11]..... 4

Figure 2.2: Recommended positions to measure (a) ball-bar and (b) flat plate in VDI/VDE 2634 part 2 [10] 5

Figure 2.3: Classification of the previous works on the calibration and performance evaluation of 3D scanners 7

Figure 4.1: Top view of the designed ball-plate (units in mm). 16

Figure 4.2: (a) Base-plate with the three V-blocks, and (b) the kinematic coupling consisting of a V-block and a support ball. 17

Figure 4.3: (a) Fabricated ball-plate without spacer and artifact's local coordinate frame, (b) ball-plate on the first spacer, (c) on the second spacer, (d) combination of the first and the second spacers, and (e) the captured 3D grid. 18

Figure 4.4: overview of the performance evaluation procedure, from artifact measurement to captured data analysis. 19

Figure 4.5: Identification marker for distinguishing sphere number 1 from sphere number 54. ... 20

Figure 4.6: Scanned point cloud of the 3D artifact 21

Figure 4.7: Errors in distance measurement. 23

Figure 4.8: Histogram of the residual distance between measured points and the fitted sphere. .. 24

Figure 4.9: Error of size measurement in various positions of the 3D grid (units in mm). 25

Figure 4.10: Errors of form measurement in various positions of the 3D grid (units in mm). 25

Figure 5.1: Schematic of followed methodology 33

LIST OF SYMBOLS AND ABBREVIATIONS

CMM	Coordinate measuirng machine

LIST OF APPENDICES

Appendix A – Darfts of the artifact's components 39

Appendix B – Reference positions of the spheres, measured by CMM, and their uncertainties...49

Appendix C – Table of Different nominal measured lengths and number of the measurements ..60

Appendix D – Designed calibration and performance evaluation artifacts in the previous works in this area 64

CHAPTER 1 INTRODUCTION

1.1 General introduction

3D scanners' development has attracted industries into using non-contact measuring devices for diverse applications, such as inspection of manufactured parts and reverse engineering purposes [1,2], instead of using contact probes. 3D scanners' faster data acquisition in comparison with touch probes is one of their advantages, which is caused by using triangulation law to determine points' locations. Two popular 3D scanning methods are laser and structured light 3D scanning.

Laser scanners include a laser source to project one or multiple laser lines on the object's surface and one or two CCDs to capture the reflected rays. 3D laser scanners measure the location of points, which are in the scanning plane of the scanner and are visible to the CCDs. Following figure shows the scanning plane in laser line scanning.

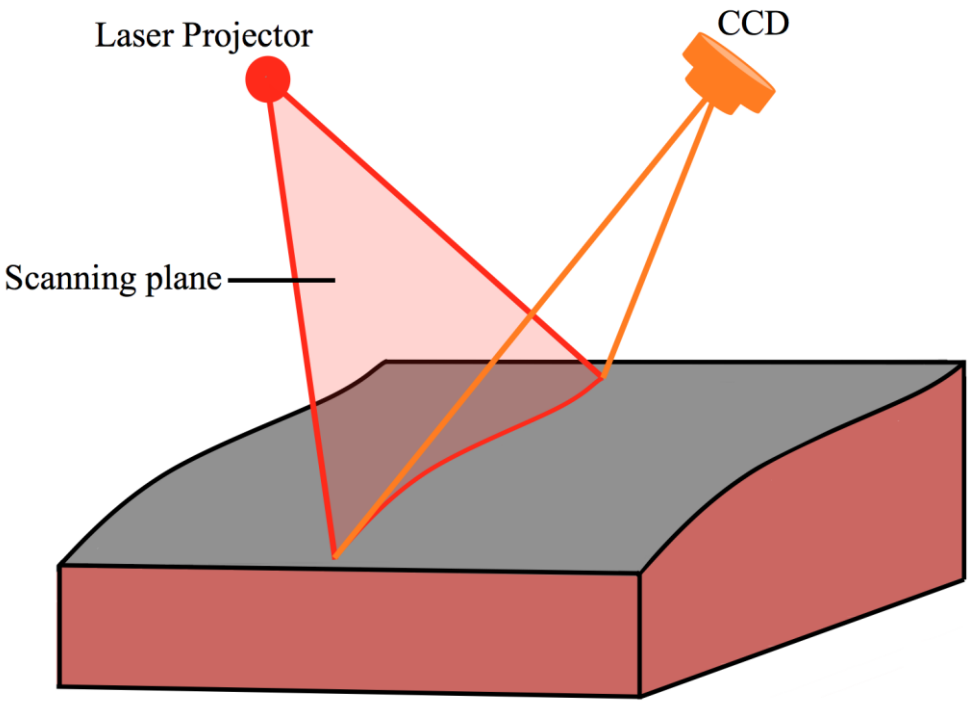

Figure 1.1: Laser scanner's scanning plane

Due to the fact that a laser scanner with one or multiple laser lines cannot cover the measurand surface, it is essential to sweep the laser scanner with respect to the measurand surface to can it.

This relative motion can be provided by a robotic arm, an operator who moves the scanner manually, or using the laser scanner as a non-contact CMM probe.

The structured light 3D scanning, which projects a pattern on the object's surface and determines the points' locations from the deformed reflected pattern [3], is the other popular 3D scanning method. Therefore, a structured light scanner comprises a projector to project the pattern on the object's surface and one or multiple cameras to capture the deformed pattern. The structured light 3D scanners are able to measure points in their scanning volume [4]. It helps the users to scan a surface in the scanner's scanning volume in one shot, with no relative motion between the surface and the scanner. It leads to faster data acquisition from a specific surface, which is one of the structured light 3D scanners' advantages in comparison with laser scanners [5,6]. The scanning volume of a structured light 3D scanner is the part of the covered volume by the projector, which is visible to the cameras. In the following figure, the blue volume is the covered volume by the scanner's projector, and the orange lines show the boundaries of the visible volume to the cameras.

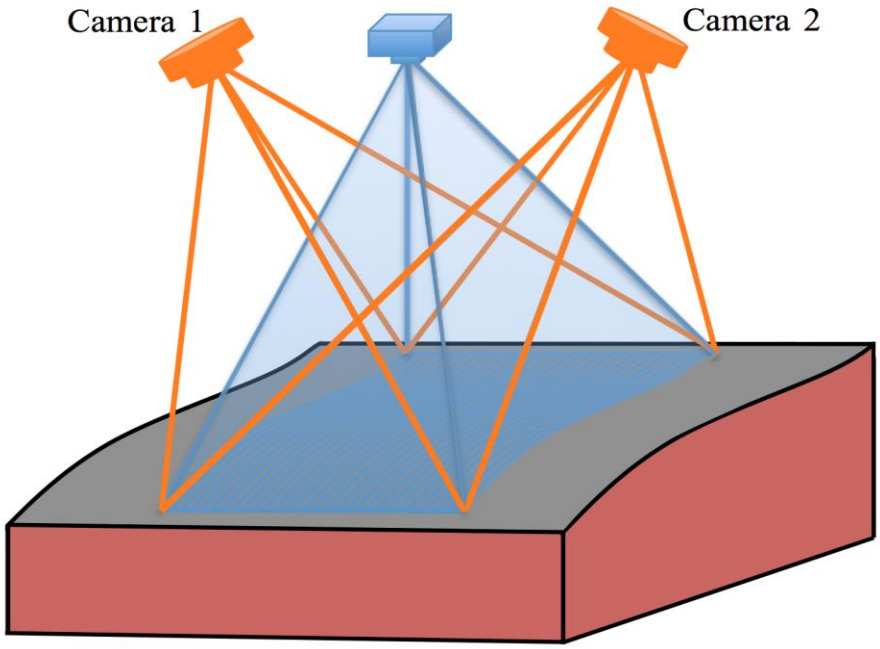

Figure 1.2: The concept of the scanning volume in structured light scanning

1.2 Problem definition

Due to spreads of non-contact measurement devices and increases in the number of the industries that are interested in using 3D scanners, specially structured light 3D scanners, 3D scanners' users need to evaluate the quality of the measured data. Also, as well as the end users, 3D scanners' developers need to find a comprehensive method to present the quality of the developed device. Therefore, both the 3D scanners suppliers and users need to find common ground, including a measurement artifact and a data analysis procedure, to present and assess the performance of the developed 3D scanner. Despite this need, no international standard is developed to evaluate the performance of the 3D scanners.

1.3 Research objective

This project aims to evaluate the metrological performance of structured light 3D scanning systems in their entire scanning volume by designing a reference artifact and developing a data analysis procedure.

1.4 Thesis outline

A literature review on the previous works in the field of performance evaluation and calibration of the laser or structured light 3D scanners is presented in the second chapter. This chapter includes an introduction of the only existing national performance evaluation standard for area-based 3D scanners, previous researches on calibration and performance evaluation of 3D scanners, two main approaches of designing reference, and limitations of these researches that need to be considered in developing a new performance evaluation guideline. The third chapter represents the research process, and the methodology followed. Chapter 4 presents the submitted paper to the journal of "Optics and Lasers in Engineering" with the title of "A pseudo-3D ball lattice artifact and method for evaluating the metrological performance of structured-light 3D scanners", and finally, chapter 5 and 6 present the general discussion and conclusion respectively.

CHAPTER 2 LITERATURE REVIEW

As the 3D scanners are gaining more popularity in different industries, the need to have a common performance evaluation guideline is felt more than before. Despite the developed international performance evaluation standards for CMM's touch [7] and non-contact [8], [9] probes, there is still no developed international standard to assess the performance of 3D scanners. The German VDI/VDE 2634 part 2 [10] is the only existing standard to evaluate the performance of 3D scanners based on area-scanning, which is not recognized as an international standard. Since it is near to impossible to model the systematic and random errors of the performance of 3D scanning systems, using reference artifacts is a valid approach to evaluate the performance of 3D scanners. Hence, different performance evaluation procedures with various reference artifacts are developed.

Using known geometrical features or free-form surfaces are two main approaches to design reference artifacts. Easy surface reconstruction from the captured point-cloud makes the known geometrical features (e.g. spheres, cylinders, and plates) popular in designing metrological artifacts. Least square fitting, which is useful in 2D and 3D, i.e., curve and surface fitting, is one of the useful methods to reconstruct the measured surfaces from a set of points. This method estimates the surface's analytical equation that minimizes the summation of the square of the residual distances between the measured points and the fitted surface or curve.

As it was mentioned, the German VDI/VDE 2634 part 2 [10] is the only existing standard to evaluate the performance of 3D scanning systems based on area scanning. A ball-bar, two spheres attached on two ends of a rigid bar, and a flat plate are two proposed artifacts in this standard, which are shown in Figure 2.1.

Figure 2.1: The used artifact to follow VDI/VDE 2634 part 2 by Erickson et al. [11]

The standard's developers asked the users to measure the ball-bar in at least seven and the flat plate in at least six different positions in the scanning volume of the scanner. Figures 2.2 (a) and (b) show the recommended measurement positions for the ball-bar and the flat plate respectively.

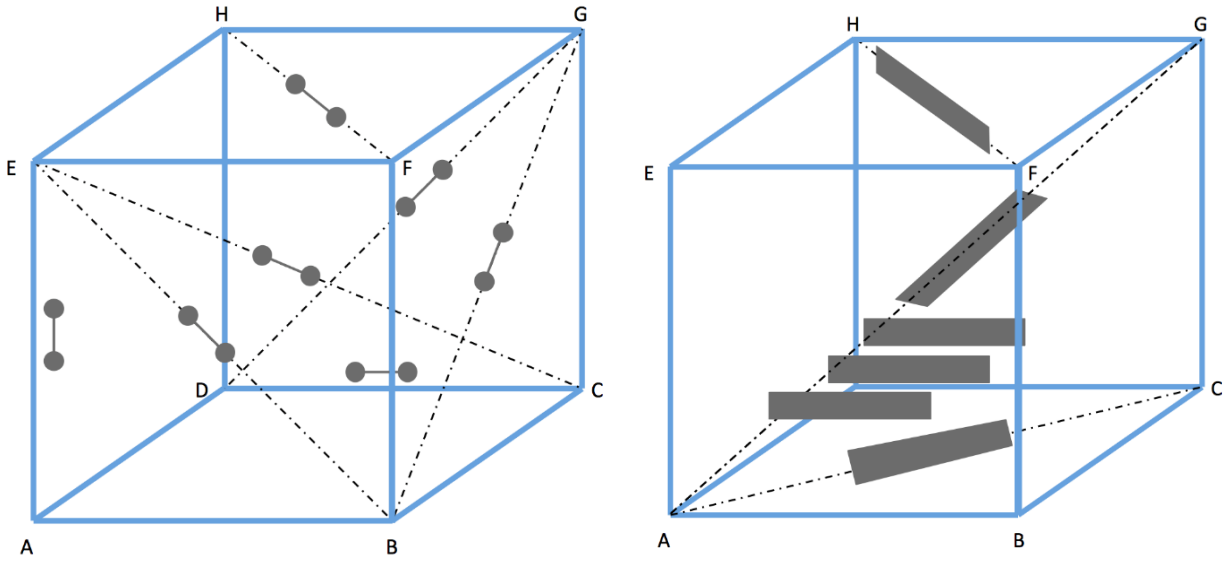

(a) (b)

Figure 2.2: Recommended positions to measure (a) ball-bar and (b) flat plate in VDI/VDE 2634 part 2 [10]

Errors in spheres' size measurement, defined as the difference between diameters of the fitted and actual spheres, error in spheres' form measurement, defined as the range of residual distances between the measured points and the fitted sphere, and sphere spacing error, defined as the difference between the measured distance between each pair of spheres the scanner data and the reference distance, are three investigated parameters in the captured point cloud by scanning the ball-bar. As the first step, a best fitted sphere with an unknown diameter should be fitted to each sphere's point cloud to investigate the errors in size and form measurements. Then, a best fitted sphere with the diameter equal to the actual diameter of spheres needs to be fitted to the spheres' point clouds to investigate the spheres' spacing error. As well as these parameters, the error in measuring the flatness of the plate is the other investigated parameter. Hence, a best fitted plane is fitted to the plate's point cloud and the range of the residual distances between the measured points and the fitted plane is reported as the inspected error in measuring the form of the plane.

Assessing the effect of newly developed calibration methods, similar to what has been done by Erickson et al. [11] and Chen et al. [12], is an example of this standard's applications.

Two of the main limitations of this performance evaluation standard are:

- Its inability to cover the scanner's scanning volume comprehensively. While 3D scanners' users need to know about the performance of their device in its entire scanning volume, these investigated parameters are studied only in some approximative positions of the scanner's field of view, which will not give a comprehensive view of what is happening in the measurement volume of the structured light 3D scanners.
- The errors in measuring the forms of spheres and planes are defined as the residual distances between the measured points and the fitted geometrical features, which is highly dependent on the number of measured points by the used 3D scanner. Thus, it cannot provide the users with a fair comparison between different 3D scanning systems with a different number of the measured points.

Beside to VDI/VDE 2634 part 2, different researchers have tried to fill this gap by designing different artifacts. Due to the similar measuring principle of laser and structured light 3D scanning systems, some of these works developed general guidelines to evaluate the performance of the triangulation based non-contact measuring devices. Iuliano et al. [13] and MacKinnon et al. [14] studied this problem by using combinations of known geometrical features such as sphere, plane, and cylinder as the measurement features. Furthermore, McCarthy et al. [15] tried to assess the performance of 3D scanners in measuring free-form surfaces by designing a free-form artifact, includes seven convex and concave spheres as the measurands, and investigating the errors in measuring distances between spheres and spheres' locations. As an example of this free-form artifact's application, Li et al. [16] have studied the effect of different ambient light conditions on the performance of a structured light 3D scanner by measuring this artifact in different light conditions.

In addition to the researches mentioned above, several performance evaluation procedures are proposed with the focus on one of these two scanning methods. Acko et al. [17] have used spheres as the main measurement feature to design a 3D tetrahedron artifact with 4 balls in the same size. The distances between each pair of spheres were studied to assess the performance of the used structured light 3D scanner. In addition to this artifact, Martínez et al. [18] have combined

cylinders, spheres, planes, and cones to design a new artifact, which was measured in multiple shots and the errors in measuring the form and size of the spheres and cylinders are examples of the investigated parameters.

Ball-plate, which is widely-used artifacts to evaluate the CMMs' performance [19], is one of the used artifacts to calibrate or assess the performance of 3D scanners. Two ball-plates with 9 and 25 balls are designed by Qiang et al. [20] and Genta et al. [21] respectively to derive the errors' trends in the performance of laser scanners. Several other artifacts, except ball-plates, are designed to evaluate laser scanner's performance. Designed artifacts by Martínez et al. [22] and Gonzalez-Jorge et al. [23] are two of these designed artifacts.

Following chart classifies different used geometrical features and investigated parameters by scanning each of them in previous works on calibration and performance evaluation of 3D scanners.

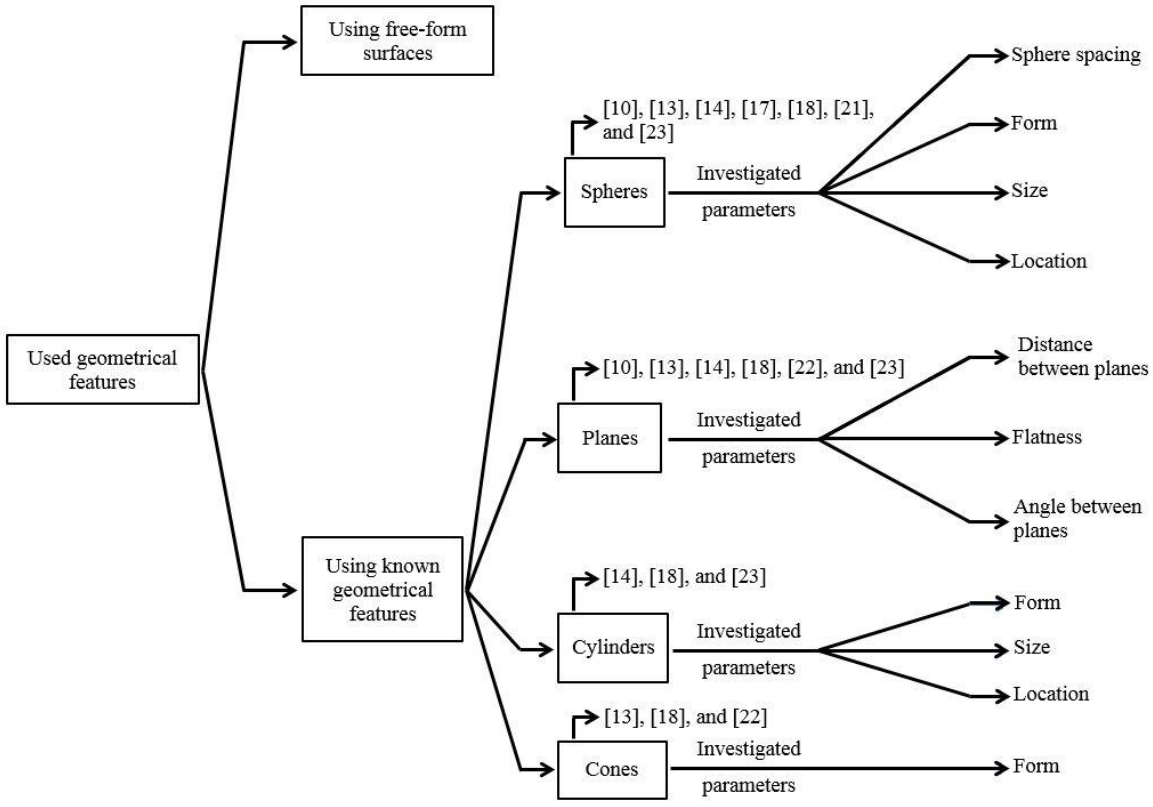

Figure 2.3: Classification of the previous works on the calibration and performance evaluation of 3D scanners

Addressing the limitations of the previously developed artifacts and data analysis procedure is the first step in developing new guidelines to assess the performance of structured light 3D scanners. One of these main limitations is the inability of the designed artifacts to cover the entire scanning volume of structured light 3D scanners. None of the proposed guidelines, even the developed guidelines by VDI/VDE 2634 part 2 [5] and Acko et al. [12] that includes measuring the measurands in limited positions of the scanner's scanning volume, are able to cover the structured light 3D scanners' scanning volume comprehensively. Also, After the artifact's fabrication and before its measurement by the scanner, its calibration is the next essential step. The fabricated artifact needs to be measured by a CMM in order to obtain the reference data, instead of using the artifact's CAD model as the reference. And finally, the investigated parameters in the proposed data analysis procedure should be independent of the measurement coordinate frames and the number of the measured points. Independency of the parameters from the measurement coordinate frame prevents the roto-translation of the scanner and reference data-sets into the same coordinate frame, which is a source of uncertainty and is affected by the scanner's performance. Also, the independency of a parameter from the number of the measured points provides a fair comparison for different 3D scanners with different numbers of measured points. Parameters such as spheres' locations and range of the residual distances between the measured points and the fitted surface, which are investigated by Genta et al. [17] and VDI/VDE 2634 part 2 [5] respectively, are examples of the investigation parameters that depends on the measurement coordinate frame and the number of the measured points.

CHAPTER 3 METHODOLOGY

The main aim of this project is to evaluate the performance of structured light 3D scanners in their scanning volume comprehensively. To achieve this goal, a pseudo-3D artifact is designed and fabricated, and a data analysis procedure is developed to process the captured point cloud by the used 3D scanner. Following steps, which are divided into three main steps, are taken to evaluate the structured light 3D scanners' performance.

3.1 Artifact design and fabrication

- Designing a metrological artifact by considering the CMM accessibility of the measurands, and mounting repeatability and stability of the artifact's structure.
- Fabricating the designed artifact from Aluminum due to its lighter weight and lower price in comparison with some widely-used alloys in fabrication of the metrological artifacts like INVAR.

3.2 Artifact measurement

- Measuring the fabricated artifact by CMM to:
    - Calibrate the fabricated artifact to obtain the reference positions of the spheres.
    - Calculate the uncertainty of the calibrated data.
- Measuring the artifact by a structured light 3D scanner to evaluate the scanner's metrological performance.

3.3 3D scanner's performance evaluation procedure

Investigating errors in size, form, and different distances measurements to provide:

- Acceptance tests for structured light 3D scanners for specific measurements with the known required accuracy.
- A comprehensive view of the performance of the 3D scanner in different positions in its scanning volume.

- Define metrics to help the guideline's users to compare the performance of two or more structured light 3D scanning systems.

CHAPTER 4 ARTICLE 1: A PSEUDO-3D BALL LATTICE ARTIFACT AND METHOD FOR EVALUATING THE METROLOGICAL PERFORMANCE OF STRUCTURED-LIGHT 3D SCANNERS

Pooya Ghandali, Farbod Khameneifar*, J.R.R. Mayer

Department of Mechanical Engineering, École Polytechnique de Montréal, Montréal, QC, Canada H3T 1J4

*Submitted to the journal of Optics and Lasers in Engineering

4.1 Abstract

This paper presents a novel reference artifact and procedure for assessing the metrological performance of structured-light 3D scanners, also known as fringe projection systems. Despite the increasing popularity of these scanners, there is still no international standard aiming at providing a guideline for how to evaluate their metrological performance. The users of the scanners, especially for part inspection, need instructions for comparing the accuracy of different systems in measuring specific parameters, as well as acceptance tests to verify whether a particular scanner can be used to inspect the part in question. As the structured-light scanners are area-scanning systems, they necessitate testing over their entire measurement volume. In order to enable this, we propose a method based on a pseudo-3D artifact calibrated by a contact probe on a coordinate measuring machine (CMM). The proposed artifact is a standard 2D ball plate that is mounted on top of spacers using kinematic couplings that ensure repeatable positioning of the ball plate with respect to the base in order to create a 3D lattice once measured. The artifact provides reference values for the distance between the centers of any pair of precision balls, as well as the reference for size and form, in order to benchmark the scanner measurements. Using the reference data, the proposed procedure enables acceptance tests and a comprehensive insight into the errors of the scanner in measuring distance, size and form at different positions within its entire scanning volume.

Keywords: 3D scanning; Structured-light scanner; Fringe projection; Metrological performance; Measurement volume; Pseudo-3D artifact

4.2 Introduction

Short-range optical 3D scanning is gaining increasing popularity in different industries, including manufacturing, for inspection and reverse engineering purposes [1,2]. Structured light scanning, also known as fringe projection technique, is one of the most popular 3D scanning technologies [3]. A structured light scanner works by projecting a series of light patterns onto the object's surface and capturing the deformed patterns by one or more cameras to determine the coordinates of points on the surface by triangulation principle [4]. The object's surface must be inside the measurement volume of the scanner (i.e., a cuboid space) in order to be scanned [5]. The ability of structured light scanner to measure points in the entire scanning volume in a single shot, while mounted on a tripod, without the need for sweeping the object's surface leads to faster data acquisition, which is one of its advantages in comparison with other scanning methods (e.g., 3D laser scanning) [6,7]. This characteristic also makes the structured light scanner an attractive option for in-process inspection of manufactured parts where the object is stationary with respect to the scanner.

End users of structured light 3D scanners need to know how to evaluate the metrological performance of their devices in order to make sure that they obtain the data they require. At the same time, suppliers of these scanners strive to find common ground with the end users in order to present and emphasize the quality of their products. For those reasons, both users and suppliers turn to standards. While international standards exist to evaluate the performance of non-contact probes on a coordinate measuring machine (CMM) [8,9], the absence of an international standard to evaluate the performance of stationary (tripod-mounted) structured light 3D scanners restricts their applications in highly regulated industries such as aerospace, where precision is of paramount importance.

The only existing standard for optical 3D scanners based on area scanning is VDI/VDE 2634 part 2 [10], a German standard, which is not recognized as an international standard. This guideline has been used as the evaluation procedure of some of the proposed calibration methods in the literature [11,12]. The standard uses a ball-bar (i.e., two spheres of the same diameters that are attached to the opposite ends of a rigid bar) and a flat plate as the measurement artifacts, and it evaluates the performance of the scanner in measuring four parameters: form and size of the sphere, flatness of the plate, and the sphere spacing. Measurements must be taken in at least 10 positions within the measurement volume of the scanner for the sphere's size and form, 7 positions for the sphere

spacing, and 6 positions for the plate's form (flatness) measurement. The range of the residuals after fitting spheres or planes to the measured points are considered the errors in measuring the form of the sphere and the flat plate, respectively. Then, the distance between the centers of the two fitted spheres is compared with the reference distance and the difference is taken as the error in measuring the sphere spacing. There are at least two limitations in the recommended procedure of the existing standard:

1. The coverage of the measuring volume in the current standard is neither comprehensive nor systematic. The evaluation of measurement errors for both form and sphere-spacing is performed in only a number of approximative positions within the scanner's field of view, while the user needs to systematically test the scanner's performance in its entire volume of measurement.

2. The error in measuring the form in the current standard depends on the number of measured points, because for both the sphere and the flat plate, the range is used as the error evaluation measure. The error value based on this measure increases monotonically as the number of points increases. Therefore, this procedure does not provide a fair comparison between different scanners and the result can be contradictory, since the scanner that gives a denser point cloud data is likely to show more errors in measuring the form according to the current standard, while it is well-known that having more points decreases the uncertainty of measurement.

Using the reference artifacts remains a valid approach for estimating the metrological performance of 3D scanners. Researchers have proposed various reference artifacts for quantifying the measurement errors of structured light scanners. As the users are able to fit analytical equations to the captured point cloud of known geometrical features such as spheres, cylinders, and plates, these features have been mostly used in the proposed artifacts [13-16]. In addition, an artifact with freeform surfaces has been presented [17]. The artifacts need to be calibrated by another instrument, which produces measurements that have, as a rule of thumb, at least an order of magnitude smaller uncertainty than the measurement uncertainty expected in the results obtained from the 3D scanner. A contact probe on a coordinate measuring machine (CMM) is generally able to give us the opportunity to calibrate an artifact with such degree of measurement uncertainty. That is why CMM measurement is used in all the available works in the literature in order to

calibrate the proposed artifacts. The CMM-based artifact calibration is deemed a reasonable way to establish the reference values. However, the overall measurement uncertainty of the artifact's reference values can be accumulated from several contributing factors including the artifact's structure, probing, etc. It is essential that the reference values provided by the artifact calibration be associated with the estimated uncertainty. Most of the above-mentioned articles do not contain uncertainty evaluations of their proposed artifacts. Most importantly, the proposed artifacts of the above works do not systematically incorporate the entire volume of measurement of the scanner.

In a related work, Genta et al. [18] have used a 2D ball-plate (i.e., a plate with 25 precision balls mounted on it) as a reference artifact for calibrating a laser scanner. The ball-plate is a well-established reference artifact in manufacturing metrology, particularly for performance verification of CMMs [19]. Genta et al. [18] measured the coordinates of the 25 ball centers once by a CMM and then by the scanner, and evaluated the performance of the scanner based on the difference between the coordinates of the ball centers in the two measurements. The comparison of the coordinates of the ball centers requires the determination of a coordinate reference system on each of the CMM data and scan data, and a rigid body transformation in order to bring the two data sets in a common coordinate frame. The coordinate reference system of the scan data is calculated based on the scanner measurement, which contains measurement errors and is a source of additional uncertainty for the evaluation procedure. Furthermore, the 2D ball plate is not best suited for the structured light scanner, because it cannot cover the entire measurement volume.

This paper extends the idea of using the well-known ball-plate and proposes a pseudo-3D ball lattice artifact and a novel systematic data analysis procedure for assessing the metrological performance of the structured light 3D scanners based on the CMM-measured reference values of the artifact. In the authors' opinion, the coordinates of the ball centers of the reference artifact should not be incorporated in the comparisons, because it makes the whole procedure prone to the inevitable errors from the defined coordinate reference system on the scan data. Instead, the coordinate measurement capability can be integrated with the distance measurement. The main advantage of using distance is being a local intrinsic quantity, as opposed to the position, which is a quantity dependent on a global coordinate system. Therefore, the distance measurement can be compared against the reference values without the need for bringing the two data sets in a common coordinate system. This way, the error of the coordinate reference system will be avoided. It is impossible to capture the entire spectrum of the measurable distances in the measuring volume, but

we can sample a large number of distance measurements if we create a 3D grid (lattice) covering the measurement volume and use the distance between any pair of grid nodes. The main philosophy behind the proposed 3D ball lattice artifact in this paper is to create that 3D grid.

The next confronted challenge is how to have a 3D lattice artifact that we can measure by the scanner without visibility problems (i.e., all the nodes should be scannable from a single point of view) and can measure by a CMM without accessibility problems (i.e., the contact probe on CMM can access all the spheres of the 3D grid). While it seems impossible to be done in 3D, it can be done in pseudo-3D fashion [20]. In this paper, we have designed a pseudo-3D artifact consisting of a ball-plate and a mechanical structure that precisely places the ball-plate in four different heights (i.e., Z-levels). The complete measurement of the artifact then gives the 3D grid, where the nodes of the 3D grid are the centers of the precision balls of the ball-plate. The precision balls of the 3D lattice are also used for assessment of the scanner's capability in measuring form and size in its entire measurement volume. Based on the devised data analysis framework, we propose strategies to be used for carrying out acceptance tests to verify whether a scanner is suitable for evaluating a tolerance of distance, size, and form.

The designed and fabricated artifact is introduced in Section 2. The proposed evaluation procedure is presented in detail in Section 3, along with the estimated uncertainty of the reference artifact. Section 4 concludes the paper.

4.3 Designed reference artifact

The basic component of the reference artifact is a ball-plate. We have chosen the plate in our work to be 180 mm long and 120 mm wide, so that the plate fits inside the measuring area of the tested commercial structured-light 3D scanner, which has the single scan range of 210 mm by 150 mm. This is approximately equal to the measuring area of several other most-widely used scanners in the market. The plate is 25.4 mm thick and is made of aluminum. The proposed design and procedure is scalable, and can be equally applied to fabricate ball-plates of larger or smaller dimensions conforming to the measuring area of the 3D scanner to be tested.

The designed ball-plate has 54 precision balls on its top face. The nominal diameter of each ball is 12.7 mm. The balls are made of aluminum oxide material, which provides us with a white scanner-friendly surface. The sphericity of the balls reported by the suppliers (i.e., Bal-tec) is 0.64 µm. The

reported ball diameter variation is also 0.64 μm. The use of a maximum possible number of balls on the ball-plate is desirable since the aim of the reference artifact is to cover the entire measuring area of the scanner with evaluation features (i.e., precision balls). However, since the artifact is measured by a contact probe on a CMM to yield the reference values, the balls must be accessible for probing by the contact probe. The probe used has a stylus tip diameter of 3 mm. Therefore, in order to be accessible, the balls are uniformly spaced in a 9 by 6 planar grid, with the distance between the center of each ball to the center of its neighboring balls in the horizontal and vertical directions of the planar grid set as 20 mm. This distance provides sufficient clearance for probing in the lateral direction. The top view of the designed ball plate is shown in the drawing of Figure 4.1.

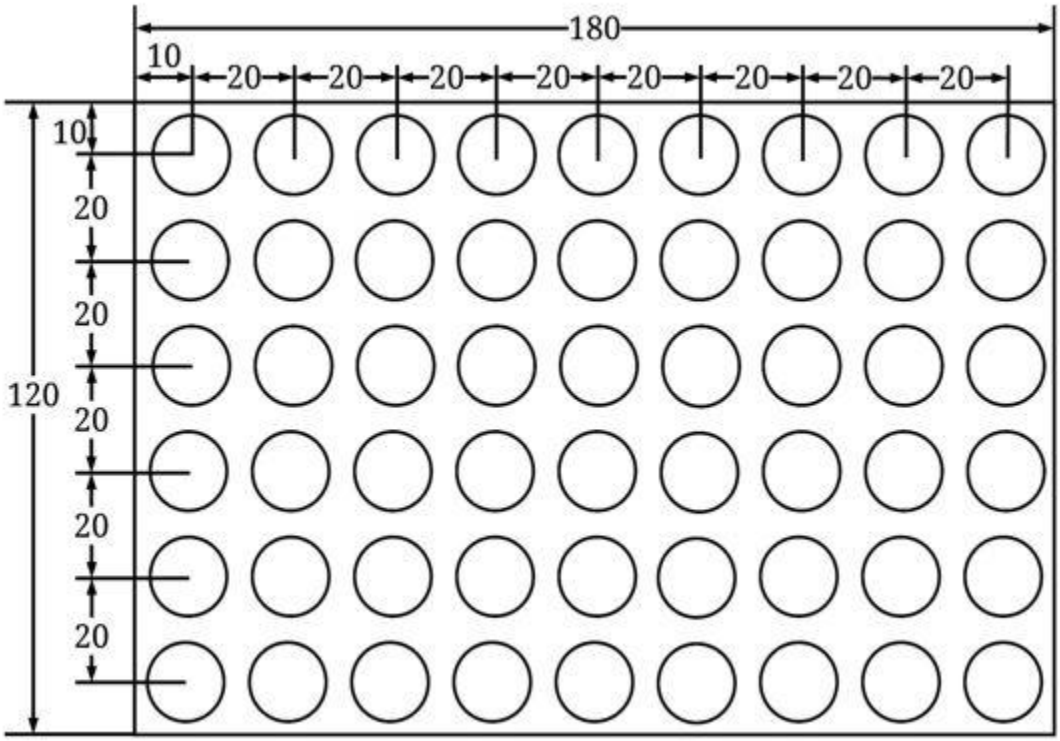

Figure 4.1: Top view of the designed ball-plate (units in mm).

In order to fabricate the ball-plate, we machined the aluminum plate to cut it into the above-mentioned dimensions, and drilled 54 blind holes (of 12 mm diameter and 5 mm depth) at the designed positions of the centers of the balls on the top surface of the plate. The machined aluminum plate initially had a shiny surface resulting in light reflections leading to outliers, thus affecting the measurement of the 3D scanner. In order to eliminate the effect of the plate's

shininess, the top surface of the fabricated plate was painted in matte black prior to gluing the 54 balls into the pre-drilled holes of the plate.

The mounting repeatability of the ball-plate is another considered design criterion. The ball plate in this work is designed with a contact interface that satisfies the principle of Exact Constraint Design [21]. In order to achieve repeatable mounting of the ball plate on the base, three pairs of kinematic couplings are utilized to constrain all six degrees of freedom of the ball plate with respect to the base. Each pair is composed of a V-block and a precision ball. For this purpose, a base plate (i.e., a flat aluminum plate) of the same size as the ball plate is fabricated. Three V-blocks are attached to the top face of the base plate as shown in Figure 4.2(a). On the back face of the ball plate, three precision balls of 12.7 mm diameter are placed in the same configuration as for the three V-blocks of the base plate. Figure 4.2 (b) shows one kinematic coupling composed of a V-block and a support ball.

(a)

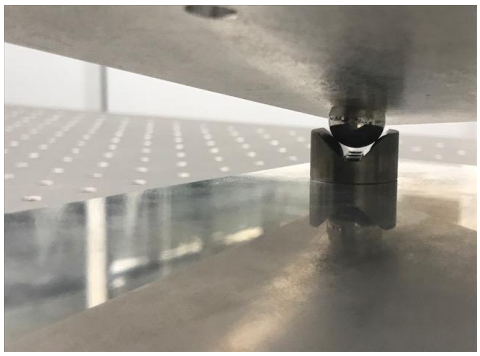

(b)

Figure 4.2: (a) Base-plate with the three V-blocks, and (b) the kinematic coupling consisting of a V-block and a support ball.

In order to create the pseudo-3D artifact that can cover the entire measuring volume of the scanner with the 3D grid, it is required to measure the ball plate at different heights with respect to the base plate. For this purpose, spacers of three different heights are designed to be inserted between the base plate and the ball plate. The concept of using spacers is inspired by the work of Bringmann et al. [20] who used a single spacer to produce a pseudo-3D artifact for testing and calibration of CNC machine tools. In our work, two spacers of 30 and 60 mm are made separately and then the height of 90 mm is obtained as the combination of these two spacers. The spacers provide a height

difference of 30 mm between each stage. The ball plate can thus be positioned not only at Z = 0 with respect to the local coordinate frame of the artifact, but also at Z = 30 mm, Z = 60 mm, and Z = 90 mm. In order to ensure mounting repeatability of the spacers, they are also kinematically coupled with the ball-plate and the base plate with three support balls of 12.7 mm diameter on one side and three V-blocks on the other side of the spacers. Figure 4.3 (a) to (d) present how different stages of the 3D grid are achieved by designed spacers and Figure 4.3 (e) illustrates the measured 3D grid, which is obtained by putting the measured data in different measuring stages together.

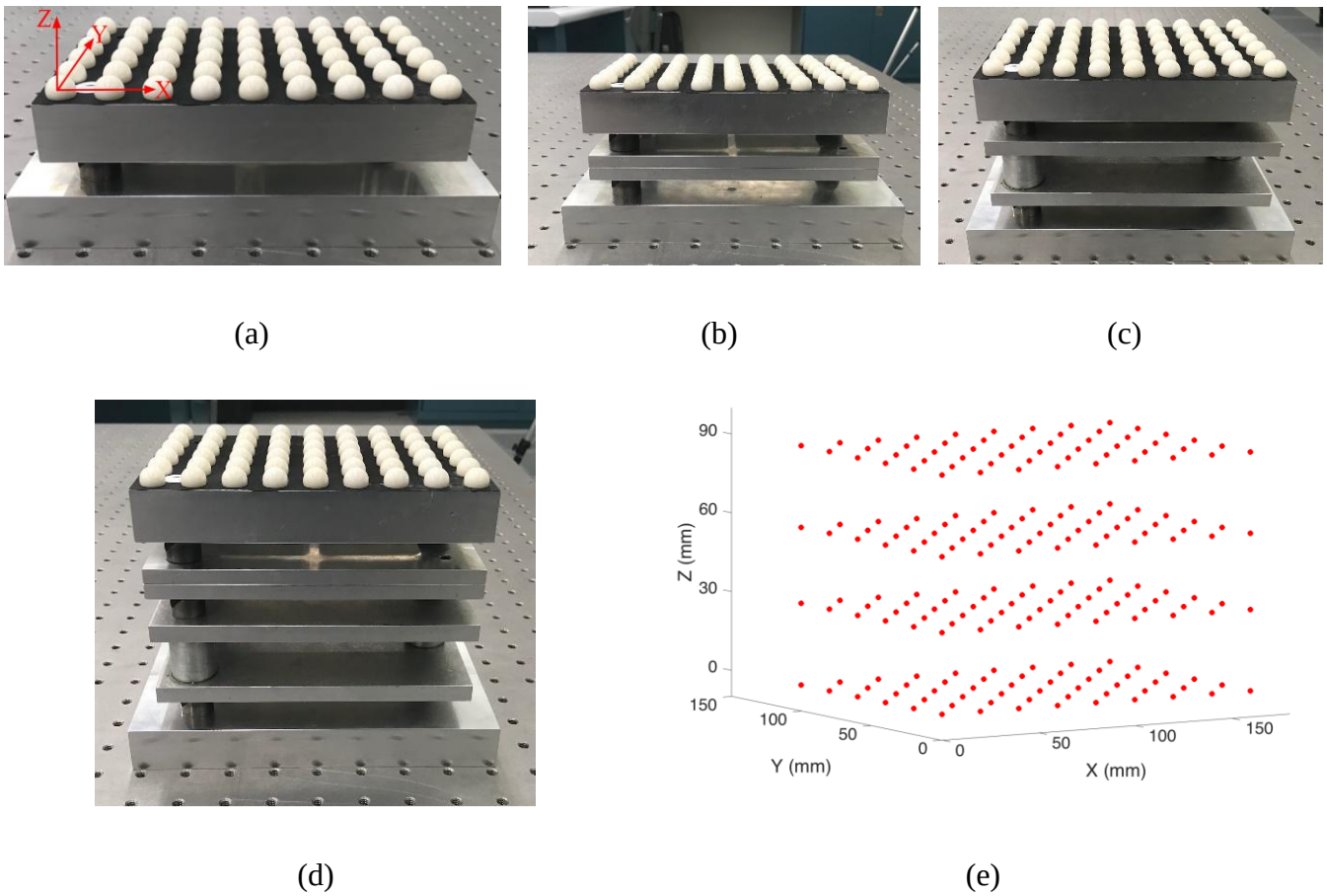

Figure 4.3: (a) Fabricated ball-plate without spacer and artifact's local coordinate frame, (b) ball-plate on the first spacer, (c) on the second spacer, (d) combination of the first and the second spacers, and (e) the captured 3D grid.

4.4 Proposed performance evaluation procedure

The overview of the proposed performance evaluation procedure and the investigated parameters are briefly illustrated in Figure 4.4. The details of each task and the parameters are discussed in the following subsections.

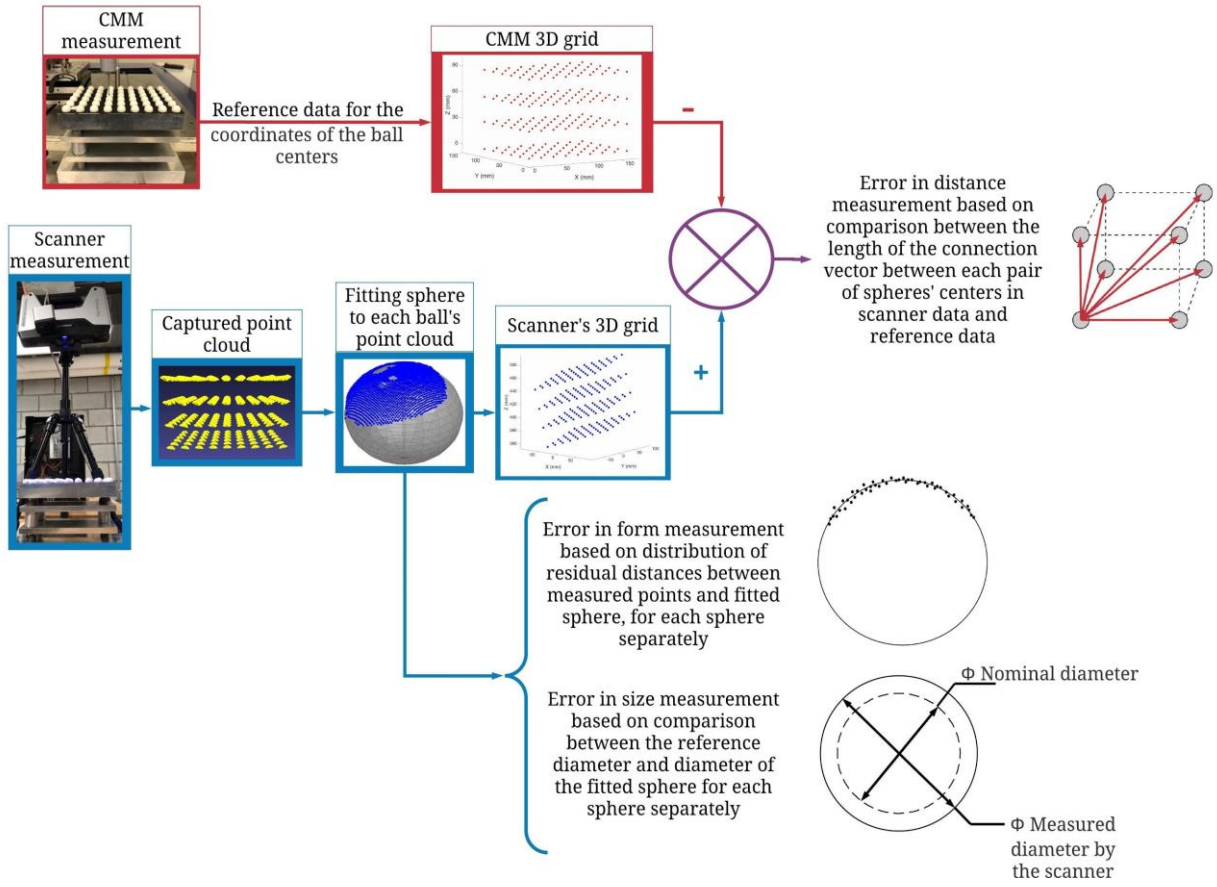

Figure 4.4: overview of the performance evaluation procedure, from artifact measurement to captured data analysis.

4.4.1 Artifact measurement

The first step of the proposed performance evaluation procedure is to calibrate the artifact using CMM measurement, in order to obtain the reference values of the 3D grid nodes (i.e., the center coordinates of balls). A Mitutoyo Legex 910 CMM equipped with a PH10M Renishaw probe is used in this work to calibrate the artifact. The ball plate mounted on stage one to four is measured

by CMM for five times and the average of these five measurements are assembled to obtain the reference data for the coordinates of the ball centers (3D grid).

Subsequently, the artifact is measured by the 3D scanner in order to evaluate the metrological performance of the scanner. Due to the symmetrical geometry of the ball plate, the identification of sphere number 1 in the scanner data is important in order to make the exact correspondence between the scan data and the CMM reference data. Knowing the correspondence between the two data sets is vital for estimating the scanning error in distance measurement, which will be discussed in detail in Section 3.2.1. In essence, there is a need for an identifier for distinguishing sphere number 1 (as marked at the bottom left of the ball plate in Figure 4.5) from sphere number 54 at the diagonally opposite corner. In this work, a white circular marker with a diameter of 15 mm is attached close to sphere number 1 in order to make it distinctive, as shown in Figure 4.5.

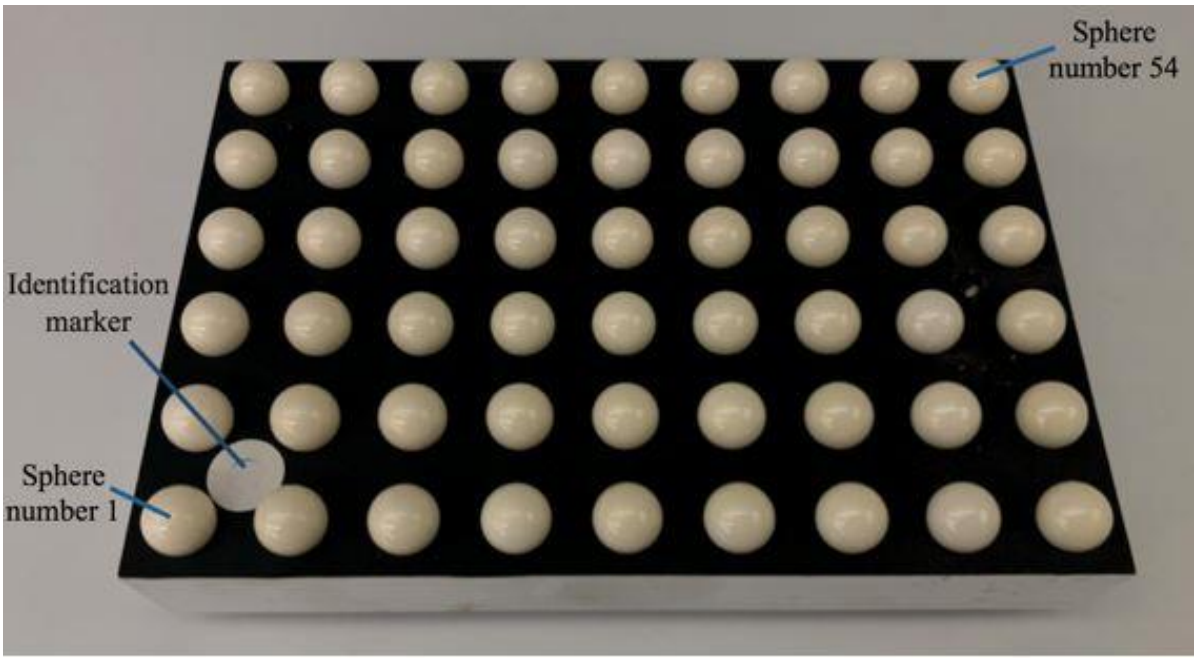

Figure 4.5: Identification marker for distinguishing sphere number 1 from sphere number 54.

An EinScan Pro structured light 3D scanner is tested in this work by the proposed artifact and procedure. The scanner, mounted on a tripod, measured the artifact. The measurement is done after performing the calibration procedure (using the calibration board) recommended by the manufacturer of the scanner. The calibration aims at providing the scanner with an accurate representation of the field of view in order to yield the best-expected performance of the measurement device.

Once each stage of the artifact is measured by the 3D scanner, the point clouds of the ball-plate in all four stages are imported to MeshLab software to remove the plate's measured points and retain the spheres' point cloud. The resulting scanned point cloud of the 3D artifact is shown in Figure 4.6.

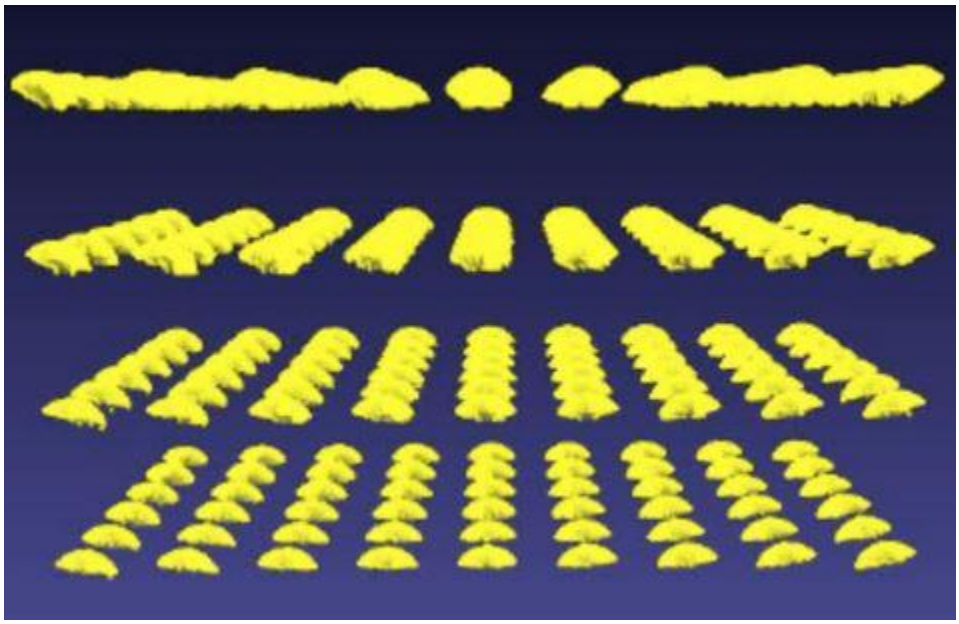

Figure 4.6: Scanned point cloud of the 3D artifact

Then, a sphere is fitted to each ball's point-cloud in order to create the 3D grid nodes (i.e., the center coordinates of balls) from the scan data. Since the outliers in data are part of the performance of the 3D scanner, no outlier is removed manually or by automatic algorithms.

Next, using the reference values for the artifact, the performance of the scanner is evaluated via the proposed investigated parameters of the next subsection.

4.4.2 Investigated parameters

Error in measuring the distances (distance between the centers of balls), error in form measurements, and error in size measurements are three investigated parameters to assess the scanner's performance. These investigated parameters are independent of the global measurement coordinate system of the scanner and the CMM data, which has the advantage of eliminating the need for roto-translation of the CMM data and scanner data to bring them to the same coordinate frame.

4.4.2.1 Error in distance measurement

In order to have a detailed evaluation of the scan data in its measuring volume, a data set as large as possible is desirable. Using the reference data for the coordinates of the ball centers (from CMM measurement), a large database of reference values for the distances of the connection vectors between ball centers are available. In essence, such a test tries to represent how well the 3D scanner can measure the distance between any two points in its measuring volume.

There are $n(n-1)/2$ unique pairs in a set of n elements, where the pairs are subject to the commutative property (i.e., AB=BA). Thus, 23,220 unique pairs are formed by connecting the 216 ball centers of the reference data (3D grid nodes created from the centers of 54 balls measured in 4 levels). The length of the line segment connecting the centers of these pairs is taken as the distance measurement feature in this work. For the designed artifact, these pairs are categorized in 143 different nominal distances. The performance of the 3D scanner in measuring these distances is assessed by comparing the length between each pair in scan data with the length between the corresponding pair in the reference data. The error in distance measurement, e_d, is then calculated for each pair as in (4.1):

$$e_{d,i} = d_{scan,i} - d_{ref,i} \tag{4.1}$$

where $d_{scan,i}$ and $d_{ref,i}$ are each measured distance in scanner data and its corresponding distance in reference data, respectively, for which the measurement error is $e_{d,i}$. For each nominal distance, measurement errors are calculated for various pairs as shown in Figure 4.7. Based on the application (i.e., the tolerance to inspect), the user knows the Maximum Permissible Error (MPE) for each distance (length) to measure. The maximum value of absolute error in measuring each distance can be compared to the MPE value as the acceptance test for the scanner whether it can be used in the inspection of the part or not. Typically, the ratio of MPE to the tolerance value is 1 to 5 or 1 to 10 [22].

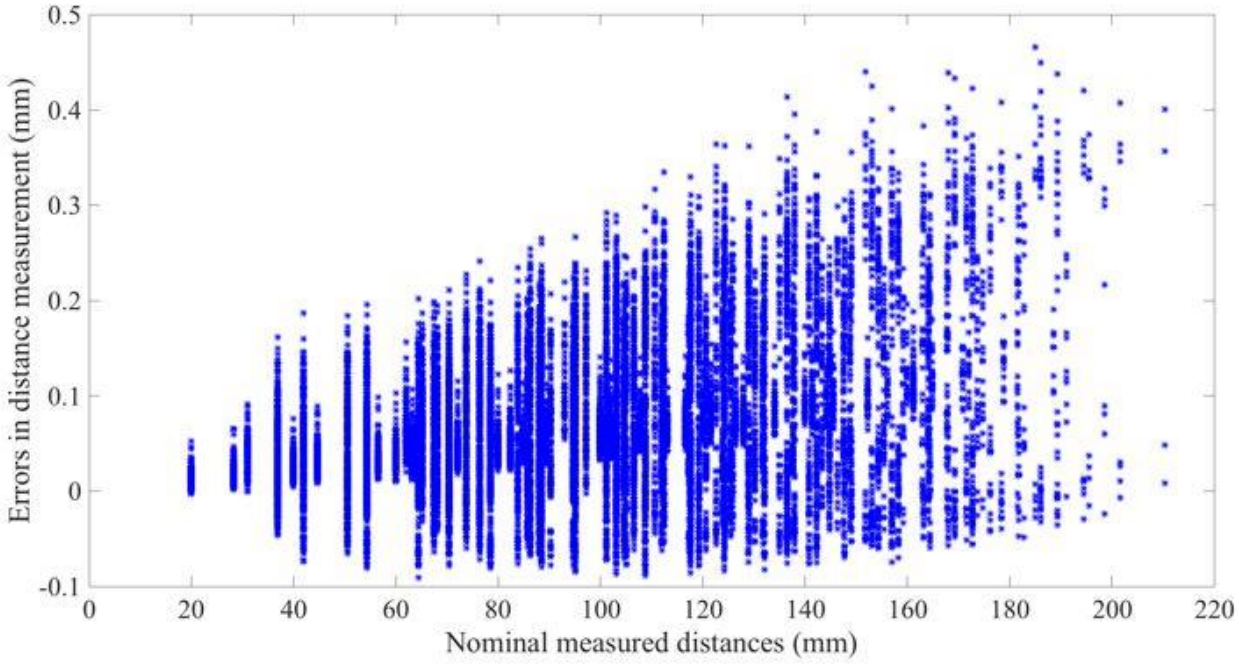

Figure 4.7: Errors in distance measurement.

The mean of absolute errors and the standard deviation of errors of distance measurement for all the 23,220 cases were calculated for EinScan Pro scanner based on the corresponding data set of Figure 4.7, and the values are respectively 0.075 mm and 0.077 mm.

4.4.2.2 Error in size and form measurement

The error in size measurement, e_s, is quantified as the difference between the diameter of the fitted sphere, D_{scan}, to the scanner's point cloud data for each ball and the ball's reference diameter, D_{ref}, reported by the supplier (Bal-tec), as in (4.2).

$$e_s = D_{scan} - D_{ref} \tag{4.2}$$

Furthermore, the residual distance between each scanned data point and the corresponding point on the fitted sphere represents the random component of error in form measurement, e_f. Since the fitted residuals closely follow a normal (Gaussian) distribution (as it can be seen in the histogram of Figure 4.8 for the scanned data), the standard deviation σ of the normal distribution can be approximated, and 3σ (which includes 99.74% of the residuals) is utilized to quantify the random error in form measurement.

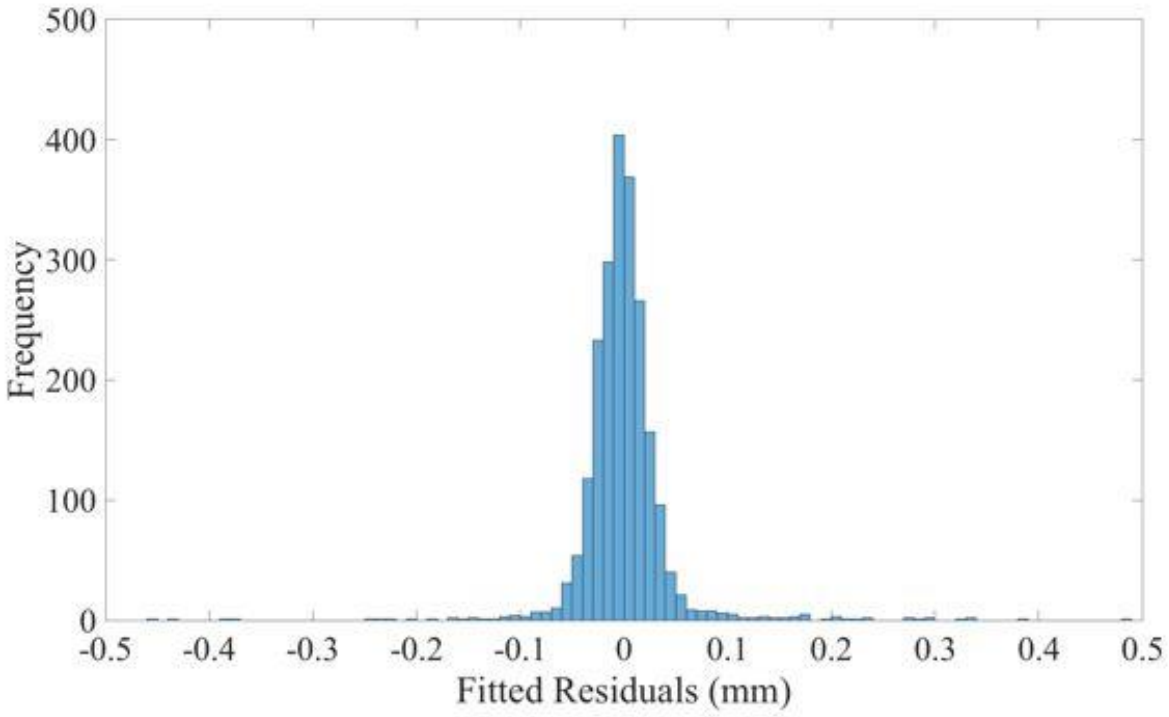

Figure 4.8: Histogram of the residual distance between measured points and the fitted sphere.

We propose that the error in size measurement (e_s) and the error in form measurement (e_f) be reported for each sphere. A colormap of the error values is shown in Figure 4.9 and Figure 4.10, which illustrates the performance of the tested 3D scanner in measuring the size and the form, respectively.

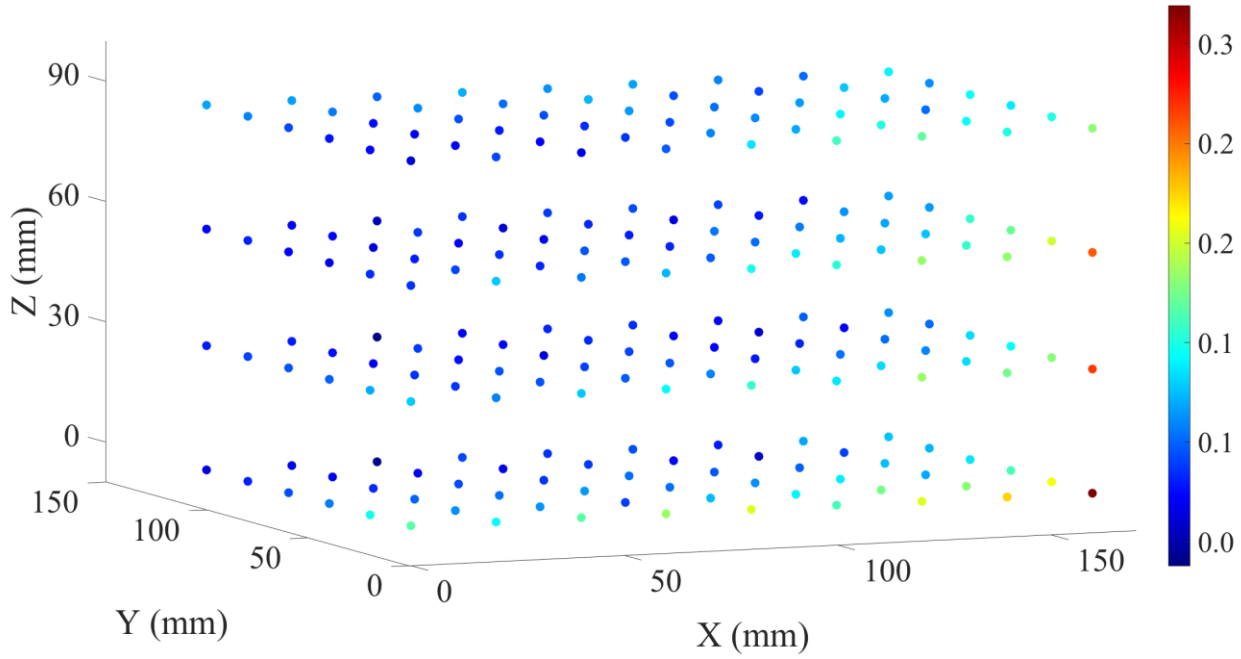

Figure 4.9: Error of size measurement in various positions of the 3D grid (units in mm).

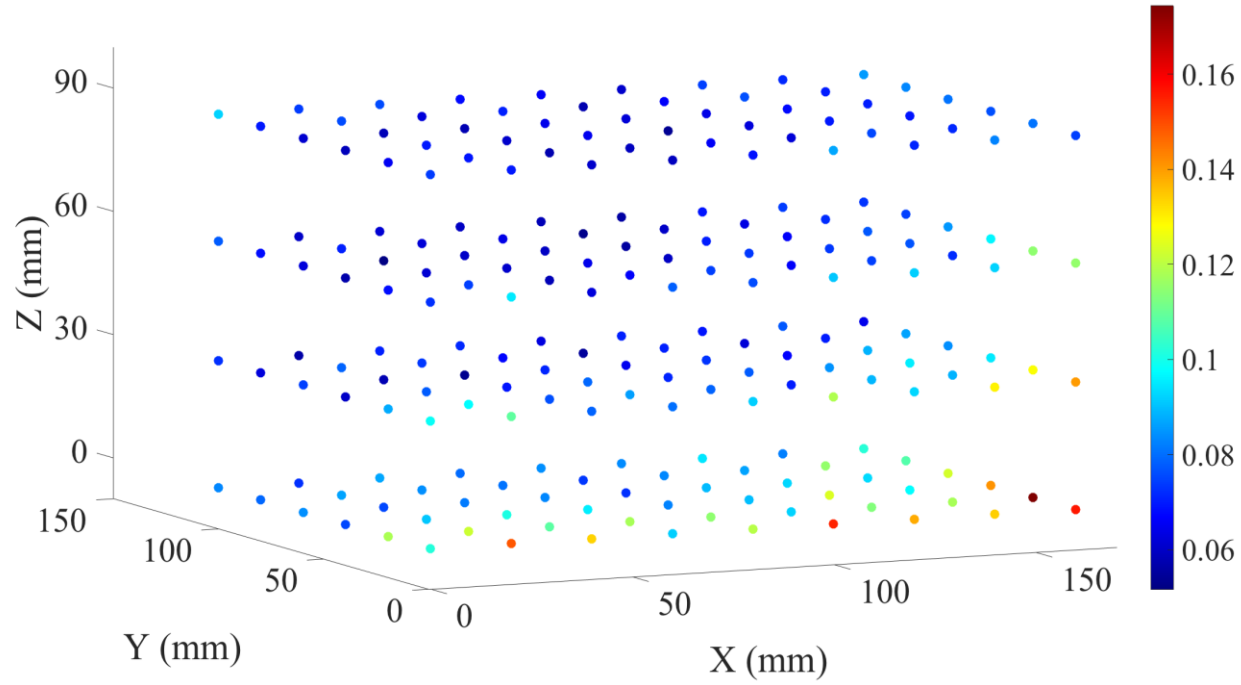

Figure 4.10: Errors of form measurement in various positions of the 3D grid (units in mm).

The colormap helps the users of a 3D scanner to have a comprehensive view of the performance of their device at different positions of its scanning volume. For example, this information could

help to determine the optimal measuring distance of the scanner from the object's surface to scan. In both cases of size and form measurement, the maximum error can be used for the acceptance test of the scanner. In addition, the mean and standard deviation of the errors in size and form measurement (of the 216 balls) is proposed to be calculated as a measure of the total performance of the scanner in its measuring volume for the size and form measurement. Tables 1 and 2 present these three values for the error in size and form measurement, respectively, for each of the 4 stages of the artifact separately, and then for the whole 3D grid. In case of the error in size measurement, since the measured diameter can be larger or smaller than the nominal diameter, the maximum and mean of the absolute errors should be reported, while the standard deviation is reported for the errors. In case of the error in form measurement, since 3σ is always a positive value, the maximum, mean and standard deviation of errors are taken into account.

Table 4.1: Error in size measurement for each level and the 3D grid (units in mm).

	Level 1	**Level 2**	**Level 3**	**Level 4**	**3D grid**
Maximum of absolute errors	0.319	0.267	0.260	0.181	0.319
Mean of absolute errors	0.121	0.104	0.106	0.111	0.111
Standard deviation of errors	0.050	0.038	0.040	0.027	0.040

Table 4.2: Error in form measurement for each level and the 3D grid (units in mm).

	Level 1	**Level 2**	**Level 3**	**Level 4**	**3D grid**
Maximum error	0.175	0.140	0.115	0.092	0.175
Mean of errors	0.102	0.080	0.071	0.069	0.081
Standard deviation of errors	0.024	0.018	0.014	0.008	0.022

4.4.3 Uncertainty of the reference data

This section presents the estimated uncertainty of the reference data for each investigated parameter. The standard uncertainty of the diameter and sphericity of the precision balls is reported by the ball supplier as 0.64 µm for both parameters. This value is regarded as the standard uncertainty of the reference data for size and form measurement (u_s and u_f, respectively). The

sources of uncertainty of the reference values of distance measurement (lengths of the connection vectors) are the CMM repeatability and the repositioning repeatability of the artifact's structure when mounting the ball plate on the spacers and the base plate through the kinematic coupling. For artifact calibration, the ball plate measurement by CMM was repeated five times from level 1 to 4, which allows the type A uncertainty calculation for estimating the uncertainty of the reference values of distance measurement [23]. From the five measured 3D grids, each connection between a pair of sphere centers is formed five times. The reference value of distance between each pair $d_{ref,i}$, is the average of five measured distances between them, which is calculated by (4.3):

$$d_{ref,i} = \frac{1}{n_j}\sum_{j=1}^{n_j} d_{i,j} \tag{4.3}$$

where a measured distance between the centers of any pair of spheres is $d_{i,j}$, and i and j are the identifiers for the i^{th} pair and the j^{th} repetition, respectively. n_j is the number of repetitions that is equal to 5 in this test.

Then, the standard deviation of the five measured distances for each pair of spheres, s_i, is calculated by (4.4).

$$s_i = \sqrt{\frac{1}{n_j - 1}\sum_{j=1}^{n_j}(d_{i,j} - d_{ref,i})^2} \tag{4.4}$$

23,220 standard deviations are formed for 23,220 measured distances, which is taken as the uncertainty of each individual reference value of distances. Finally, a pooled standard deviation is calculated by (4.5) for all reference values of distances together, and regarded as the standard uncertainty of the reference data for distance measurement, u_d. In (4.5), n_i is the number of the measured distances, which is equal to 23,220. The pooled standard deviation of the measured distances, yielded by (4.5), is 1.45 µm.

$$u_d = \sqrt{\frac{1}{\sum_{i=1}^{n_i}(n_j - 1)}\sum_{i=1}^{n_i}(n_j - 1){s_i}^2} \tag{4.5}$$

Table 3 summarizes the standard uncertainty and the expanded uncertainty $U = ku$ with the coverage factor $k = 2$ (corresponding to a coverage probability of approximately 95%) for the reference values of the three investigated parameters.

Table 4.3: The uncertainty of the reference data for the investigated parameters.

	Reference for distance	**Reference for size**	**Reference for form**
Standard uncertainty	1.45 µm	0.64 µm	0.64 µm
Expanded uncertainty U (k = 2)	2.90 µm	1.28 µm	1.28 µm

4.5 Conclusions

Evaluation of the metrological performance of structured light 3D scanners is essential for the applications of part inspection and quality control in manufacturing. Currently, there is no international standard for assessing these 3D scanners. A novel performance evaluation procedure has been proposed in this paper based on a pseudo-3D ball lattice reference artifact, which allows the simultaneous coverage of the measurement volume of the scanner for quantifying the errors in measuring three parameters, namely distance, size, and form. The three-dimensional grid generated by measuring the proposed artifact consists of 216 nodes that are centers of the balls. There are thus 23,220 unique pairs of nodes, the distance between which can be categorized in 143 nominal distances. The artifact provides a reference value for the distance between each of the unique pairs, which is a rich database for evaluating the performance of the scanner in measuring different distances (lengths) in its measuring volume. Furthermore, the 216 precision balls yield reference data for assessing the capability of the scanner in measuring size and form at different positions in the scanning volume. A first version of the artifact has been built. The expanded uncertainty of the reference data is estimated to be 2.90 µm (k = 2) for distances, and 1.28 µm (k = 2) for size and form. The developed data analysis procedure provides the users with acceptance tests for the 3D scanner, and a comprehensive view of the errors of the 3D scanner in measuring distance, size, and form in its measurement volume.

4.6 Acknowledgments

The authors would like to acknowledge the financial support of the Natural Sciences and Engineering Research Council of Canada (NSERC) through the Discovery Grants program.

4.7 References

[1] Zhang S. Handbook of 3D machine vision: optical metrology and imaging. Series in optics and optoelectronics. Hoboken, NJ: CRC Press; 2013.

[2] Stavroulakis PI, Leach RK. Invited review article: review of post-process optical form metrology for industrial-grade metal additive manufactured parts. Rev Sci Instrum 2016;87:041101.

[3] Wang Z, Nguyen DA, Barnes JC. Some practical considerations in fringe projection profilometry. Opt Lasers Eng 2010;48:218–25.

[4] Gorthi SS, Rastogi P. Fringe projection techniques: whither we are? Opt Lasers Eng 2010;48:133–40.

[5] Luhmann T, Wendt K. Recommendations for an acceptance and verification test of optical 3-D measurement systems. Int Arch Photogramm Remote Sens 2000;XXXIII:493–500.

[6] Van der Jeught S, Dirckx JJJ. Real-time structured light profilometry: a review. Opt Lasers Eng 2015;87:18–31.

[7] Zhang S. High-speed 3D shape measurement with structured light methods: a review. Opt Lasers Eng 2018;106:119–31.

[8] ISO 10360-7:2011. Geometrical product specifications (GPS) - acceptance and verification tests for coordinate measuring machines (CMM) - Part 7: CMMs equipped with imaging probing systems; 2011.

[9] ISO 10360-8:2013. Geometrical product specifications (GPS) - acceptance and verification tests for coordinate measuring machines (CMM) - Part 8: CMMs with optical distance sensor; 2013.

[10] VDI/VDE 2634-2. Optical 3D measuring systems: optical systems based on area scanning; 2012.

[11] Chen R, Xu J, Ye Z, Li J, Guan Y, Chen K. Easy-to-operate calibration method for structured light systems. Appl Opt 2016;55:8478–85.

[12] Eiríksson ER, Wilm J, Pedersen DB, Aanæs H. Precision and accuracy parameters in structured light 3-D scanning. Int Arch Photogramm Remote Sens Spat Inf Sci 2016;XL-5/W8:7–15.

[13] Iuliano L, Minetola P, Salmi A. Proposal of an innovative benchmark for comparison of the performance of contactless digitizers. Meas Sci Technol 2010;21:105102.

[14] Acko B, McCarthy M, Haertig F, Buchmeister B. Standards for testing freeform measurement capability of optical and tactile coordinate measuring machines. Meas Sci Technol 2012;23:094013.

[15] MacKinnon D, Carrier B, Beraldin JA, Cournoyer L. GD&T-based characterization of short-range non-contact 3D imaging systems. Int J Comput Vis 2013;102:56–72.

[16] Martínez-Pellitero S, Cuesta E, Giganto S, Barreiro J. New procedure for qualification of structured light 3D scanners using an optical feature-based gauge. Opt Lasers Eng 2018;110:193–206.

[17] McCarthy MB, Brown SB, Evenden A, Robinson AD. NPL freeform artefact for verification of non-contact measuring systems. Int Soc Opt Photonics 2011:78640K.

[18] Genta G, Minetola P, Barbato G. Calibration procedure for a laser triangulation scanner with uncertainty evaluation. Opt Lasers Eng 2016;86:11–19.

[19] Kunzmann HI, Trapet E, Waldele F. Results of the international comparison of ball plate measurements in ClRP and WECC. CIRP Ann - Manuf Technol 1995;44:479–82.

[20] B. Bringmann, A. Kung WK. A measuring artefact for true 3D machine testing and calibration. CIRP Ann - Manuf Technol 2005;54:471–74.

[21] Slocum A. Kinematic couplings: a review of design principles and applications. Int J Mach Tools Manuf 2010;50:310–27.

[22] Brown & sharpe. Understanding the ISO 10360-2 performance standard. North Kingstown; 2001.

[23] GUM. Evaluation of measurement data — Guide to the expression of uncertainty in

measurement. Joint Committee for Guides in Metrology (JCGM); 2008.

CHAPTER 5 GENERAL DISCUSSION

This research proposed a novel guideline, including a metrological artifact and a data analysis procedure, to fill the lack of an international performance evaluation standard for structured light 3D scanning systems. Due to the ability of the structured light 3D scanners in measuring points in their scanning volume in a single shot, as shown in Figure 1.2, the focus of this work is on assessing the performance of a 3D scanner in its entire scanning volume. Hence, a metrological artifact has been designed to obtain a pseudo-3D grid as the measurement result. The designed artifact includes a ball-plate, 54 aluminum oxide spheres with the diameter of 12.7 mm glued on an aluminum plate, and three aluminum spacers, which are responsible to move the ball-plate in the direction of the plate's normal vector for four different stages. The CAD model of the designed artifact and drafts of the designed and used components are presented in Appendix A. Stability and mounting repeatability of the artifact's components and accessibility of the measurement features for the touch of the CMM probe are considered criteria in the designed artifact.

Firstly, the fabricated artifact was measured five times from level one to four by a Mitutoyo Legax 910 CMM. The measured positions of the spheres and the uncertainties of these measurements are reported in Appendix B for each sphere separately. Therefore, the connection vectors between each pair of spheres were formed five times. The average of these five measured lengths is used as the reference length of each vector, totally 23,220 vectors. The uncertainty of the reference lengths, which is the pooled of standard deviations of all the 23,220 measured lengths, is calculated equal to 1.45 micron.

After the artifact's calibration, it was measured by a structured light 3D scanner. The captured point cloud of each stage was imported to MeshLab software in order to remove measured points of the plate and to separate the spheres' point clouds. Then, a best fitted sphere was fitted to each sphere's point cloud to determine the center position and radius of each sphere in the 3D scanner's data-set.

The errors in measuring size, form, and various distances are investigated parameters, which are independent of the measurement coordinate frame and numbers of the measured points. Errors in measuring various distances and errors in form measurement are two investigated parameters by ISO 10360-2 [2], the international CMM performance evaluation standard, too. Beside these two parameters, the error in size measurement is the other investigated parameter in this proposed performance evaluation procedure. Following figure illustrates the followed methodology briefly.

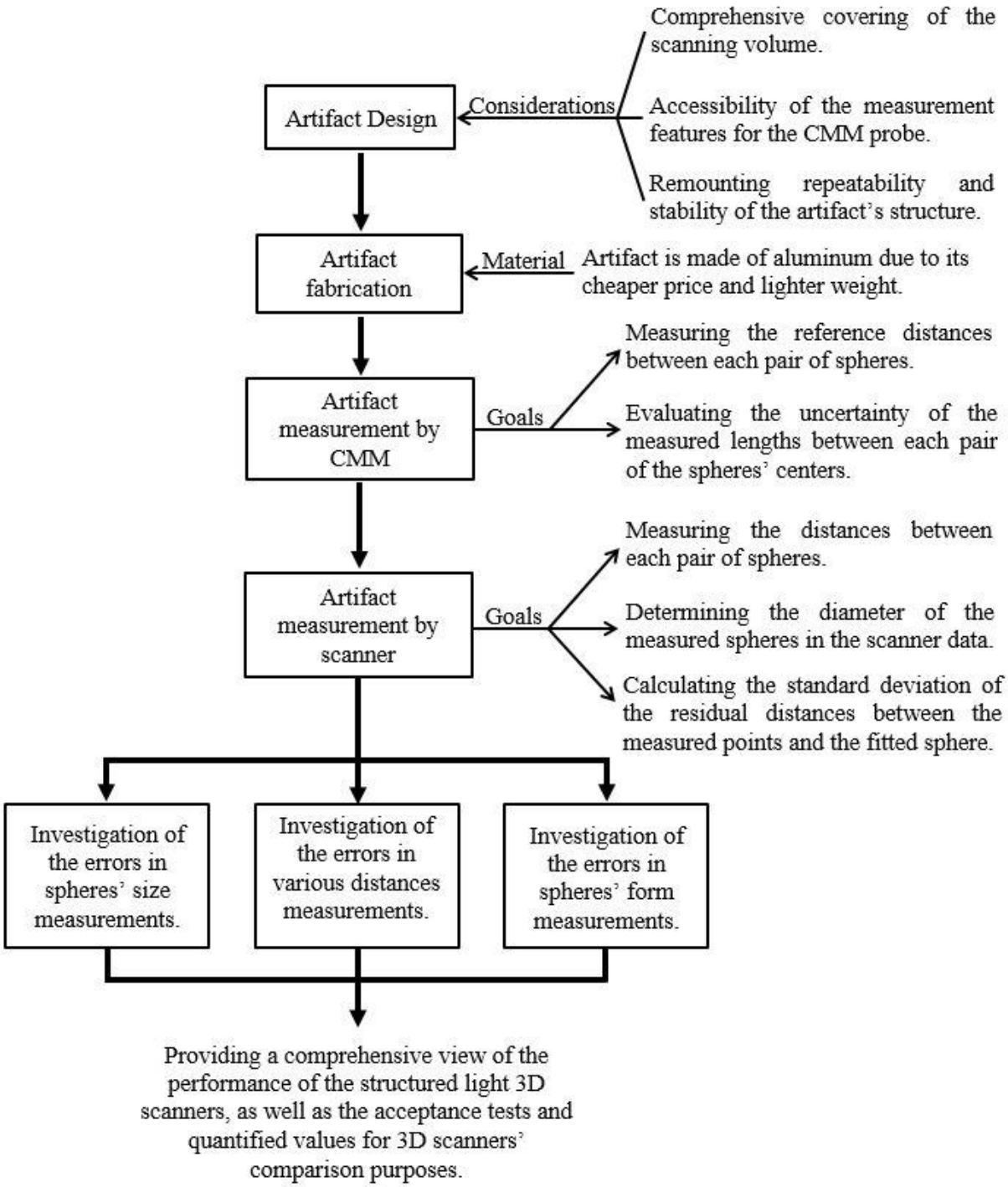

Figure 5.1: Schematic of followed methodology

As a case study, an EinScan Pro structured light 3D scanner was used to scan the artifact and follow the proposed data analysis procedure in order to evaluate the 3D scanner's performance. Therefore, the performance of the used structured light 3D scanner is assessed as follow:

- In the case of assessing the performance of the structured light 3D scanner in measuring various distances, 23220 distances, categorized in 143 specific cases, were measured. These 143 cases and the number of each case's measurement are reported in Appendix C. The errors in measuring different distances are reported in Figure 4.7. This data-set is useful as an acceptance test to see if the used 3D scanner meets the requirements to inspect a specific manufactured part, based on the tolerances of the part, or not.
- The errors in measuring size and form are the other investigated parameter. Figure 4.9 and Figure 4.10 represent the errors in measuring the size and form of the spheres respectively. These two figures give the users a comprehensive view over the performance of the scanner in 216 different positions of its scanning volume. Moreover, Table 4.1 and Table 4.2 have reported the maximum error, mean of errors, and standard deviation of the errors for each level and whole 3D grid.

The mean of the absolute errors and the standard deviation of the errors, for each parameter separately, are calculated to provide the guideline's users with metrics to describe the performance of the structured light 3D scanner. Following table presents the maximum error, mean of the errors, and standard deviation of the errors in measuring each parameter separately.

Table 5.1. Maximum error, mean of the absolute errors, and standard deviation of the errors in measuring each parameter

	Errors measuring in various distances	$\|\Delta D\|$	3σ
Maximum error	0.175	0.140	0.115
Mean of absolute errors	0.102	0.080	0.071
Standard deviation of the errors	0.024	0.018	0.014

CHAPTER 6 CONCLUSION AND RECOMMENDATIONS

Despite the 3D scanners' advantages, the absence of an international performance evaluation standard causes skepticism regarding the performance of the 3D scanners in industries with needs of high accuracy measurements. This project has focused on assessing the performance of structured light 3D scanners in their entire scanning volume by designing and fabricating a pseudo-3D artifact, as the reference artifact, and developing an algorithm to analyze the captured data. Errors in size, form, and various distance measurements are investigated in the captured data, due to their independence from the measurement coordinate frame and the number of the measured points for each sphere. The proposed performance evaluation procedure provides the structured light 3D scanners' users and manufacturers with acceptance tests and a comprehensive view on the performance of the 3D scanner in different positions of its scanning volume.

The recommended future works are as follows:

- In this work, the accuracy of a single scan has been studied. The next step is to assess the influence of stitching multiple scans, as it is the case in scanning a complete object.
- In the current work, not outliers have been removed from the captured point cloud data. The proposed procedure can be used to investigate the effect of different point cloud data processing algorithms (e.g., outlier removal algorithms) on the accuracy of data.
- An important factor in 3D scanning an object is the ambient light. In the current work, we kept the ambient light conditions constant. As a future work, it is interesting to study the effect of ambient light conditions on the accuracy of the data.
- An interesting future topic to pursue is to make another version of the artifact with spheres of different sizes, materials, and colors to assess the influence of them on the accuracy of scan data.

BIBLIOGRAPHY

[1] S. Zhang, Handbook of 3D Machine Vision: Optical Metrology, Hoboken, NJ: CRC Press, 2013.

[2] P. I. Stavroulakis and R. K. Leach, “Invited Review Article: Review of post-process optical form metrology for industrial-grade metal additive manufactured parts,” *Rev. Sci. Instrum.*, vol. 87, no. 4, 2016.

[3] S. S. Gorthi and P. Rastogi, “Fringe projection techniques: Whither we are?,” *Opt. Lasers Eng.*, vol. 48, no. 2, pp. 133–140, 2010.

[4] T. Luhmann and K. Wendt, “Recommendations for an Acceptance and Verification Test of Optical 3-D Measurement Systems,” *Int. Arch. Photogramm. Remote Sens.*, vol. XXXIII, no. February, pp. 493–500, 2000.

[5] S. Van der Jeught and J. J. J. Dirckx, “Real-time structured light profilometry: A review,” *Opt. Lasers Eng.*, vol. 87, pp. 18–31, 2015.

[6] S. Zhang, “High-speed 3D shape measurement with structured light methods: A review,” *Opt. Lasers Eng.*, vol. 106, no. December 2017, pp. 119–131, 2018.

[7] ISO, "ISO 10360-2. Geometrical product specifications (GPS) - Acceptance and reverification tests for coordinate measuring machines (CMM)- Part 2: CMMs used for measuring linear dimensions", 2009.

[8] ISO, "ISO 10360-7. Geometrical product specifications (GPS) - Acceptance and verification tests for coordinate measuring machines (CMM)- Part 7: CMMs equipped with imaging probing systems", 2011.

[9] ISO, "ISO 10360-8. Geometrical product specifications (GPS) - Acceptance and verification tests for coordinate measuring machines (CMM)- Part 8: CMMs with optical distance sensor", 2013.

[10] Verein Deutsche Ingeieure, "VDI/VDE 2634-2. Optical 3D measuring systems: Optical systems based on area scanning", 2012.

[11] E. R. Eiríksson, J. Wilm, D. B. Pedersen, and H. Aanæs, “Precision and Accuracy Parameters in Structured Light 3-D Scanning,” *Int. Arch. Photogramm. Remote Sens. Spat.*

Inf. Sci., vol. XL-5/W8, no. December 2015, pp. 7–15, 2016.

[12] R. Chen, J. Xu, Z. Ye, J. Li, Y. Guan, and K. Chen, "Easy-to-operate calibration method for structured light systems," *Appl. Opt.*, vol. 55, no. 30, pp. 8478–8485, 2016.

[13] L. Iuliano, P. Minetola, and A. Salmi, "Proposal of an innovative benchmark for comparison of the performance of contactless digitizers," *Meas. Sci. Technol.*, vol. 21, no. 10, 2010.

[14] D. MacKinnon, B. Carrier, J. A. Beraldin, and L. Cournoyer, "GD&T-based characterization of short-range non-contact 3D imaging systems," *Int. J. Comput. Vis.*, vol. 102, no. 1–3, pp. 56–72, 2013.

[15] M. B. McCarthy, S. B. Brown, A. Evenden, and A. D. Robinson, "NPL freeform artefact for verification of non-contact measuring systems," *Int. Soc. Opt. Photonics*, vol. 7864, no. January 2011, p. 78640K, 2011.

[16] F. Li, D. Stoddart, and I. Zwierzak, "A Performance Test for a Fringe Projection Scanner in Various Ambient Light Conditions," *Procedia CIRP*, vol. 62, pp. 400–404, 2017.

[17] B. Acko, M. McCarthy, F. Haertig, and B. Buchmeister, "Standards for testing freeform measurement capability of optical and tactile coordinate measuring machines," *Meas. Sci. Technol.*, vol. 23, no. 9, 2012.

[18] S. Martínez-Pellitero, E. Cuesta, S. Giganto, and J. Barreiro, "New procedure for qualification of structured light 3D scanners using an optical feature-based gauge," *Opt. Lasers Eng.*, vol. 110, no. June, pp. 193–206, 2018.

[19] H. I. Kunzmann, E. Trapet, and F. Waldele, "Results of the International Comparison of Ball Plate Measurements in ClRP and WECC," *CIRP Ann. - Manuf. Technol.*, vol. 44, pp. 479–482, 1995.

[20] Z. Qiang and W. Wei, "Calibration of laser scanning system based on a 2D ball plate," *Meas. J. Int. Meas. Confed.*, vol. 42, no. 6, pp. 963–968, 2009.

[21] G. Genta, P. Minetola, and G. Barbato, "Calibration procedure for a laser triangulation scanner with uncertainty evaluation," *Opt. Lasers Eng.*, vol. 86, pp. 11–19, 2016.

[22] S. Martínez, E. Cuesta, J. Barreiro, and B. Álvarez, "Methodology for comparison of laser digitizing versus contact systems in dimensional control," *Opt. Lasers Eng.*, vol. 48, no. 12,

pp. 1238–1246, 2010.

[23] H. Gonzalez-Jorge, B. Riveiro, E. Vazquez-Fernandez, J. J. Martínez-Sánchez, and P. Arias, "Metrological evaluation of Microsoft Kinect and Asus Xtion sensors," *Meas. J. Int. Meas. Confed.*, vol. 46, no. 6, pp. 1800–1806, 2013.

APPENDICES

APPENDIX A – DARFTS OF THE ARTIFACT'S COMPONENTS

This appendix presents the drafts of the artifact's components. In the following pages the draft of the base plate, the reference plate of the ball plate, bottom and top plate of the first spacer, bottom and top plate of the second spacer, the used aluminum tube to connect two plate in the second spacer, the used V-block, VB-375-SM, and the used sphere, 500-TBR-T, which is going to be coupled with the V-block. Following figure shows the CAD model of the designed artifact. The parts' numbers are indicated in this figure and the following drafts are in this order.

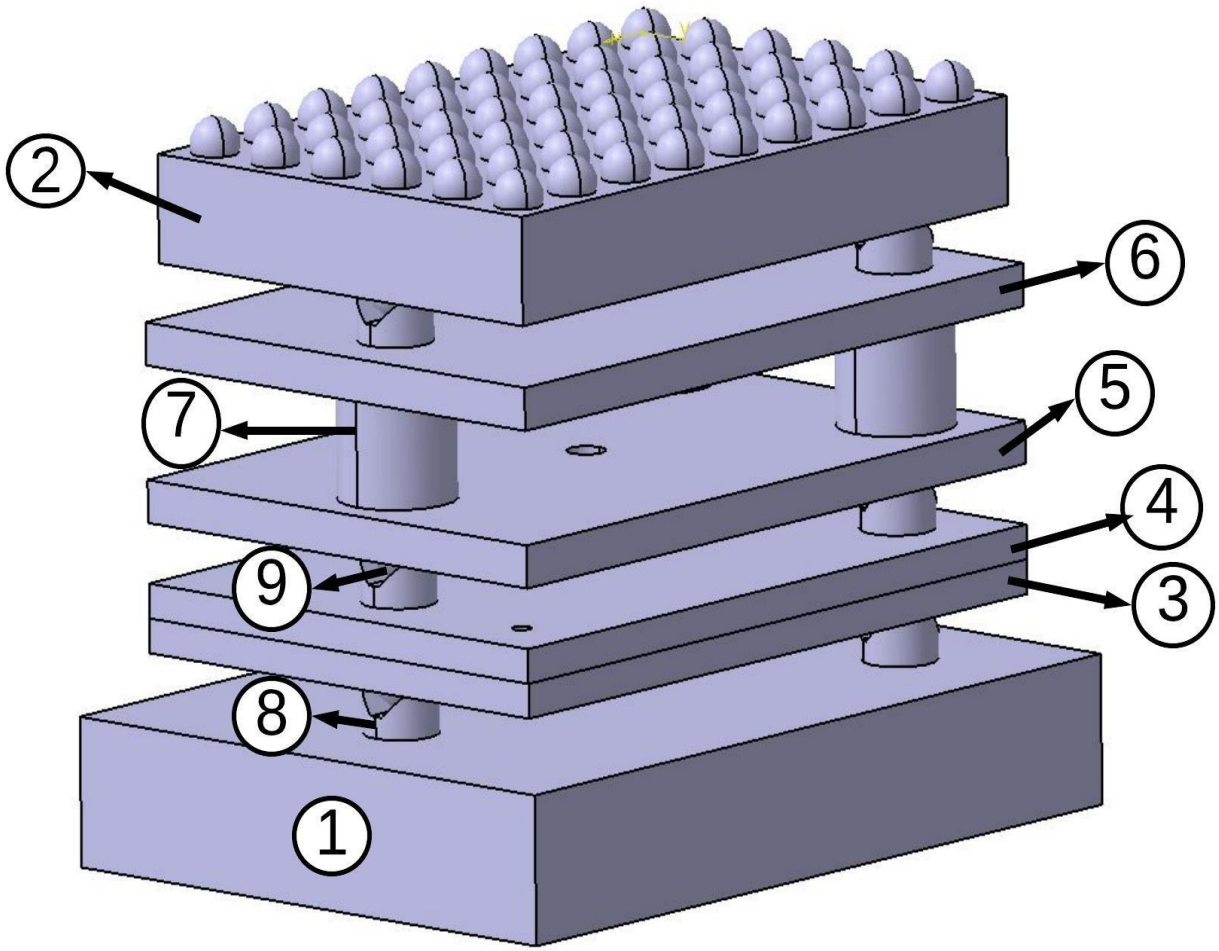

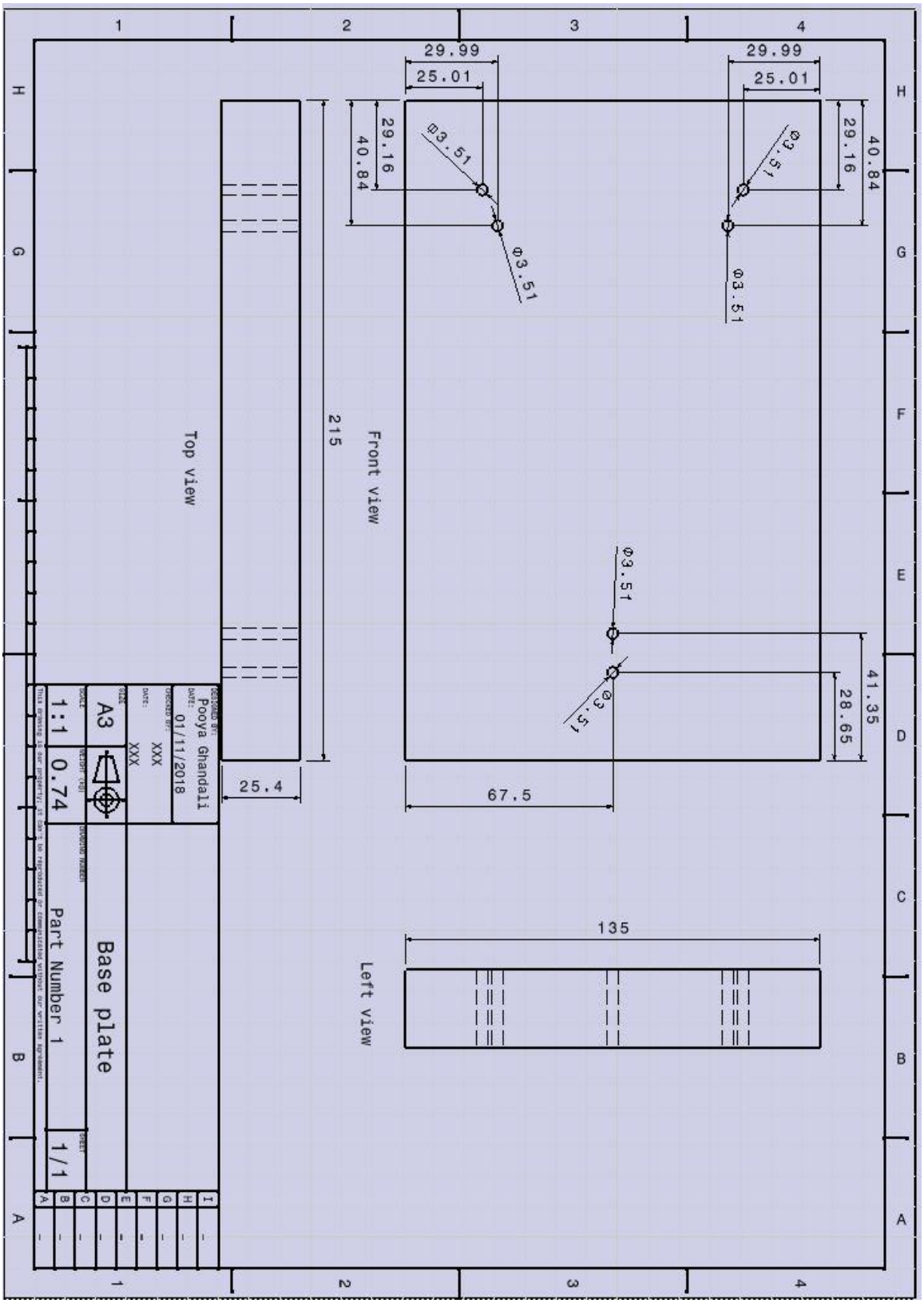
29.99
25.01
29.16
40.84
Φ3.51
Top view
Front view
Left view
215
25.4
67.5
135
41.35
28.65
Base plate
Part Number 1
A3
1:1
0.74
1/1
Pooya Ghandali
01/11/2018
XXX

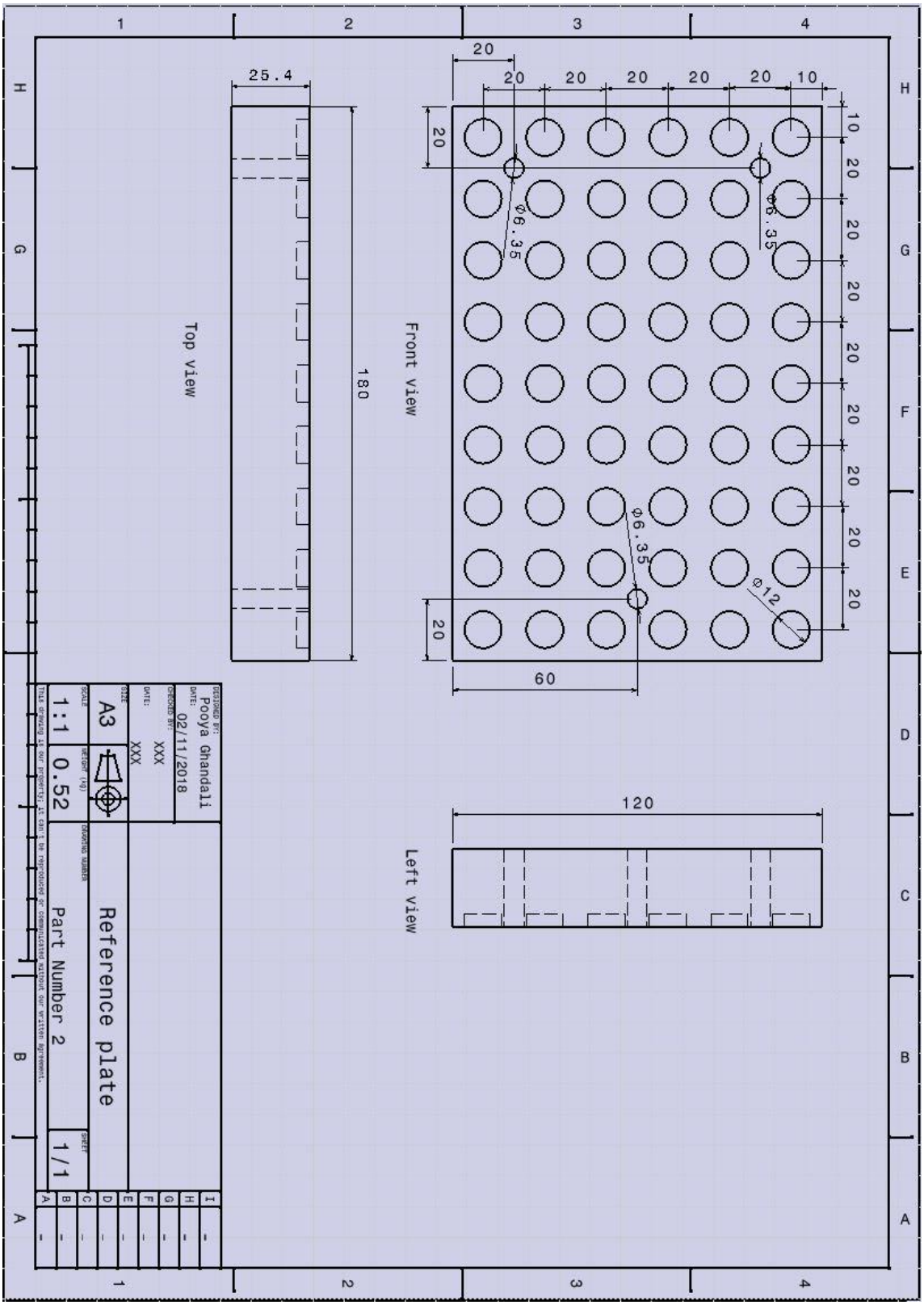
Top view
Front view
Left view
25.4
180
120
60
20
10
Ø6.35
Ø12
Reference plate
Part Number 2
Pooya Ghandali
02/11/2018
XXX
A3
1:1
0.52
1/1

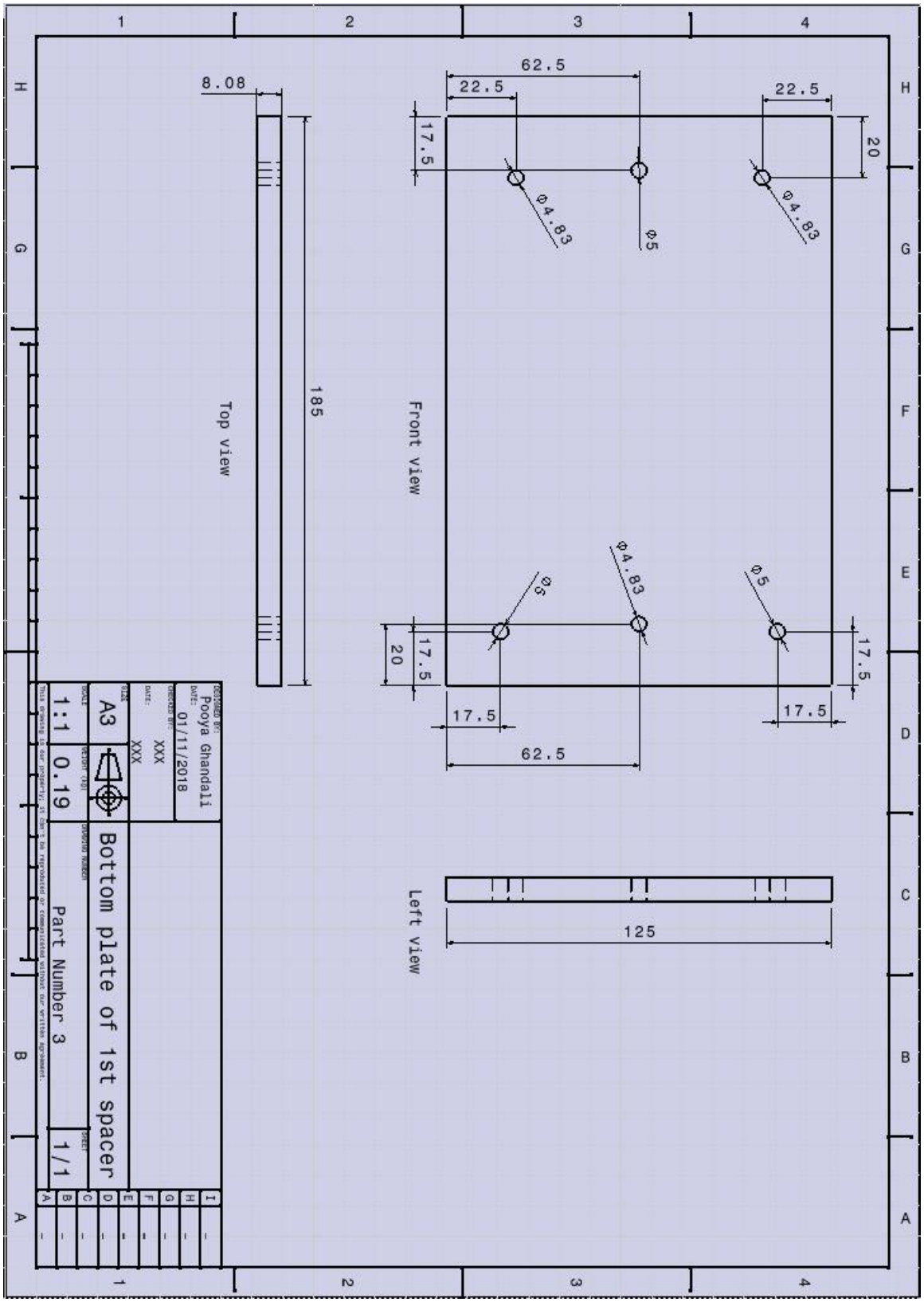
Top view
8.08
185
Front view
62.5
22.5
22.5
17.5
20
Φ4.83
Φ5
Φ4.83
Φ5
Φ4.83
Φ5
20
17.5
17.5
17.5
17.5
62.5
Left view
125
DESIGNED BY: Pooya Ghandali
DATE: 01/11/2018
CHECKED BY: XXX
DATE: XXX
SIZE A3
SCALE 1:1
WEIGHT (kg) 0.19
DRAWING NUMBER Part Number 3
SHEET 1/1
Bottom plate of 1st spacer

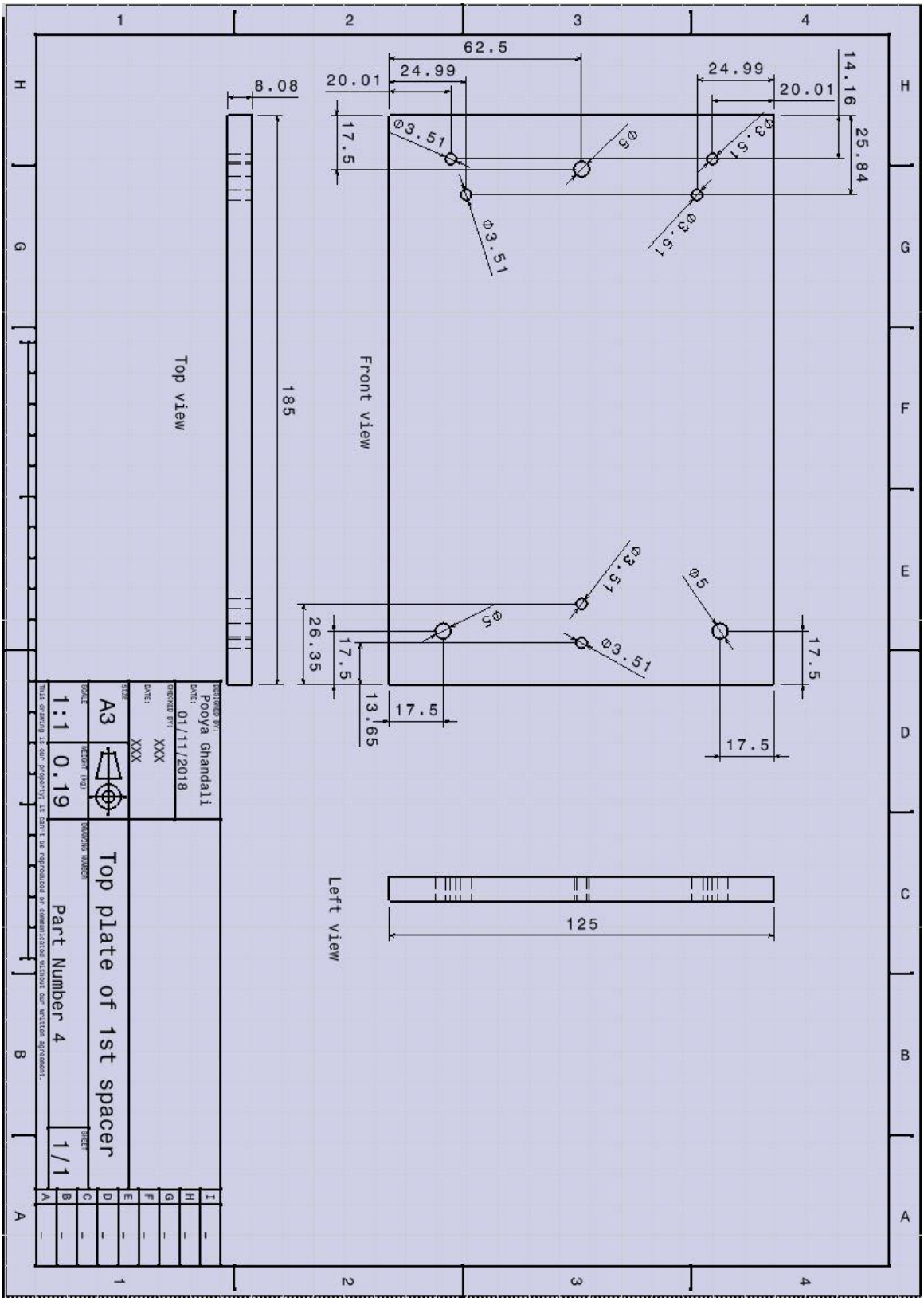
62.5
24.99
20.01
8.08
24.99
20.01
14.16
25.84
17.5
Ø3.51
Ø5
Ø3.51
Ø3.51
Ø3.51
Top view
185
Front view
Ø3.51
Ø5
Ø5
Ø3.51
26.35
17.5
17.5
13.65
17.5
17.5
Left view
125
DRAWN BY: Pooya Ghandali
DATE: 01/11/2018
CHECKED BY: XXX
DATE: XXX
SIZE A3
SCALE 1:1
WEIGHT (kg) 0.19
DRAWING NUMBER Part Number 4
SHEET 1/1
Top plate of 1st spacer
This drawing is our property. It can't be reproduced or communicated without our written agreement.

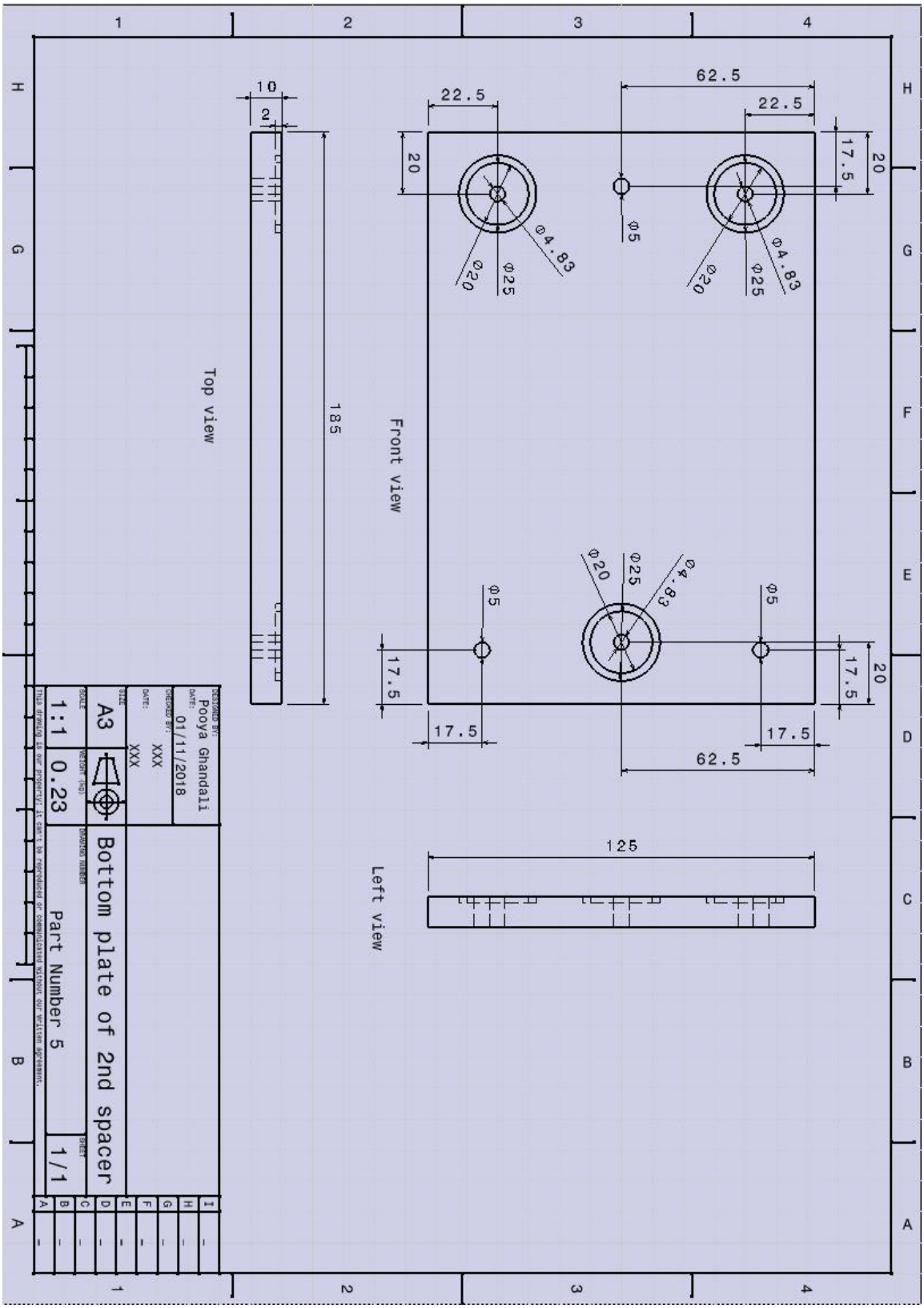
Top view
Front view
Left view
10
2
185
22.5
62.5
22.5
20
17.5
20
Φ5
Φ4.83
Φ20
Φ25
Φ4.83
Φ20
Φ25
Φ20
Φ25
Φ4.83
Φ5
Φ5
17.5
17.5
20
17.5
17.5
62.5
125
DESIGNED BY: Pooya Ghandali
DATE: 01/11/2018
CHECKED BY: XXX
DATE: XXX
SCALE 1:1
WEIGHT (kg) 0.23
SIZE A3
DRAWING NUMBER Part Number 5
SHEET 1/1
Bottom plate of 2nd spacer

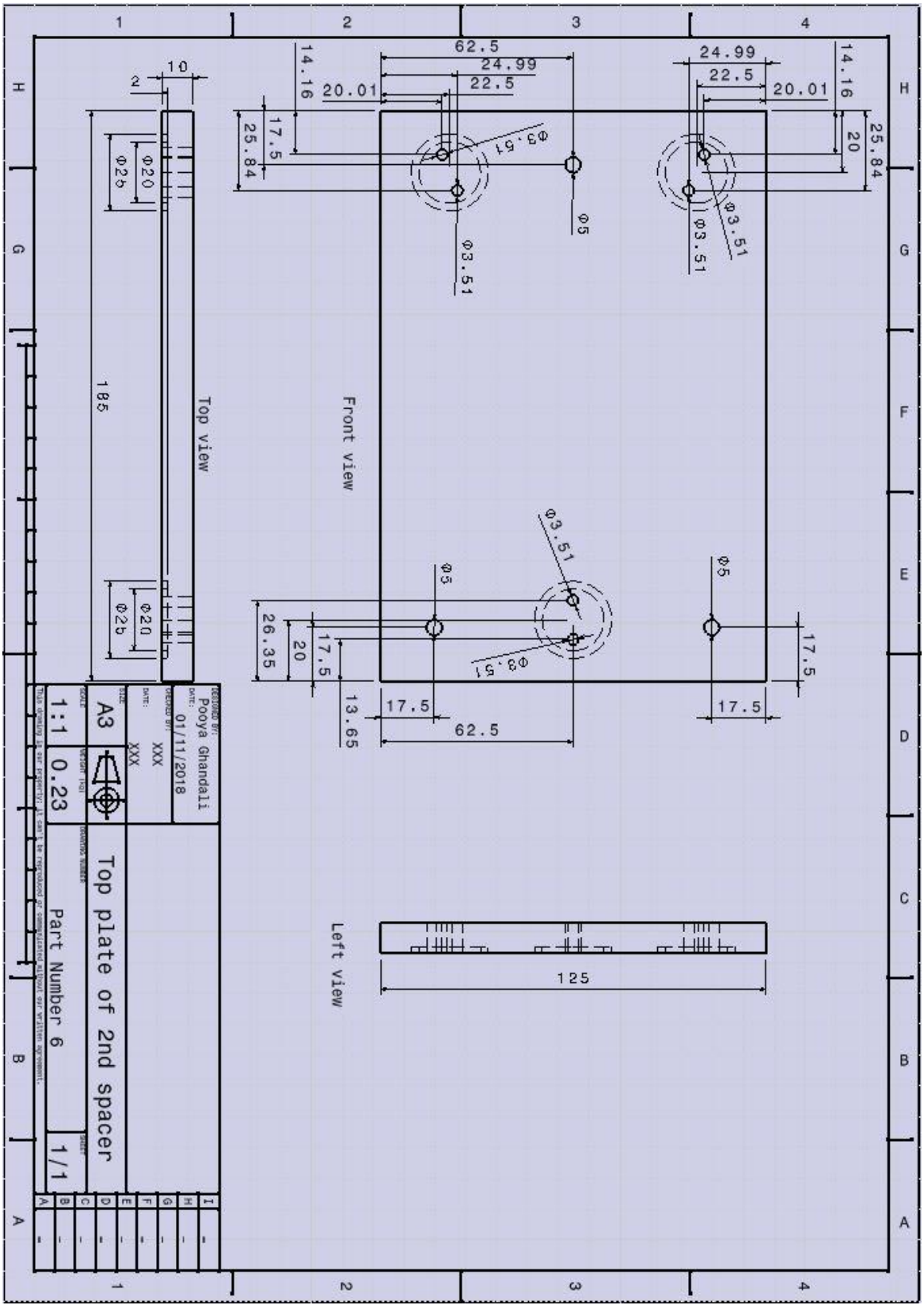
Top view
Front view
Left view
Φ3.51
Φ5
Φ20
Φ26
185
125
62.5
24.99
22.5
20.01
14.16
25.84
17.5
20
26.35
13.65
Pooya Ghandali
01/11/2018
XXX
A3
1:1
0.23
Top plate of 2nd spacer
Part Number 6
1/1

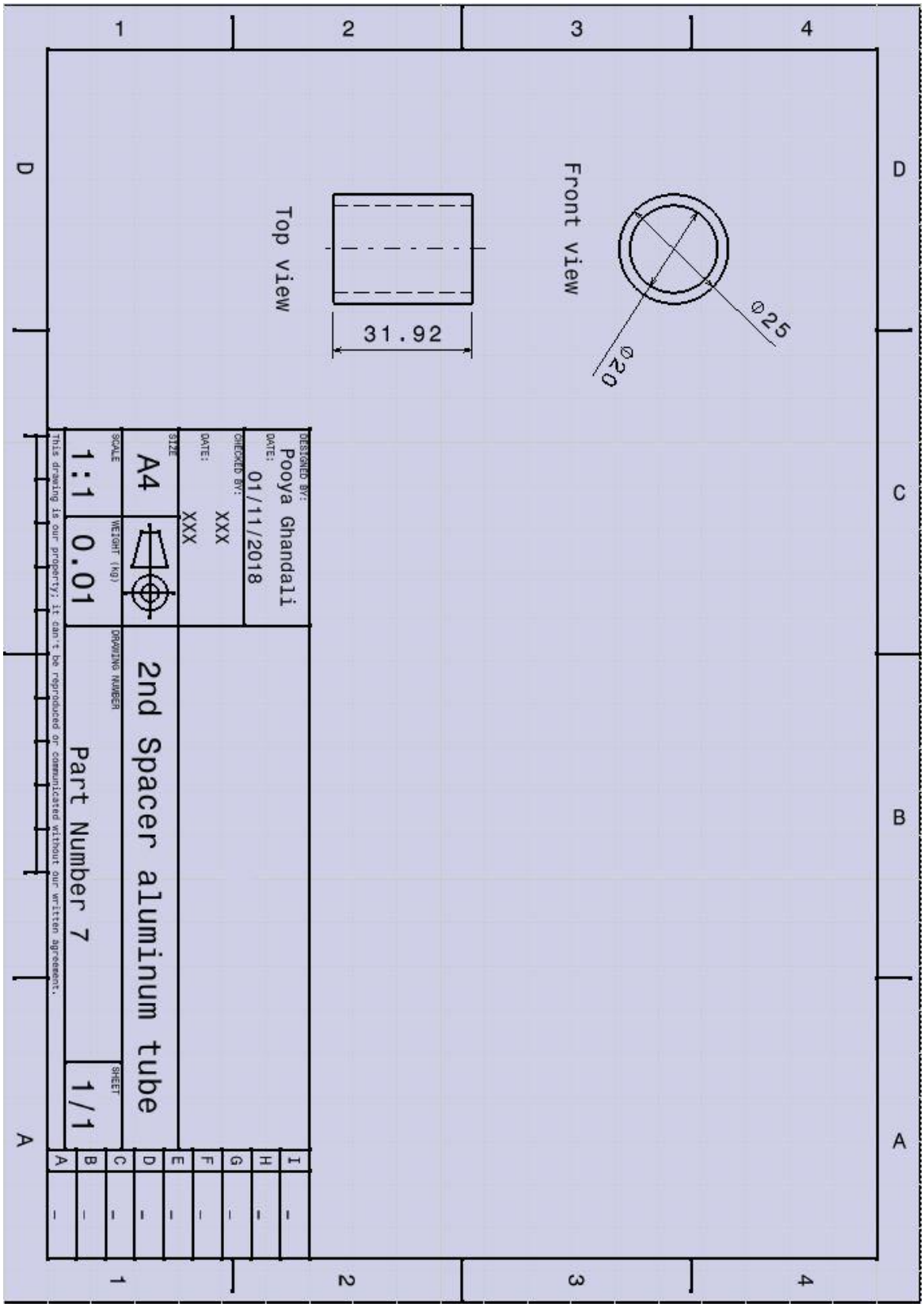
Top view
31.92
Front view
Ø25
Ø20
DESIGNED BY:
Poova Ghandali
DATE:
01/11/2018
CHECKED BY:
XXX
DATE:
XXX
SIZE
A4
SCALE
1:1
WEIGHT (KG)
0.01
DRAWING NAMBER
Part Number 7
SHEET
1/1
2nd Spacer aluminum tube
This drawing is our property; it can't be reproduced or communicated without our written agreement.

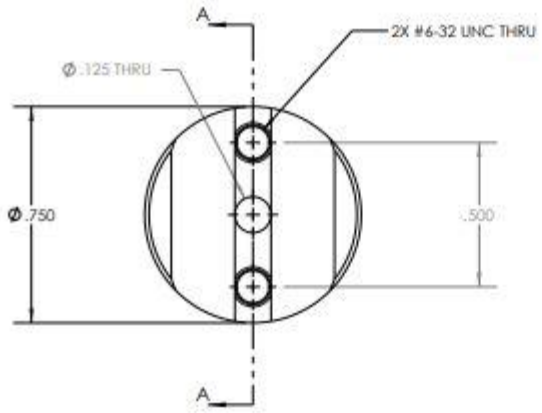

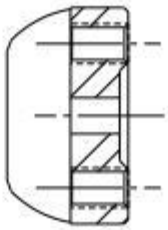

SECTION A-A

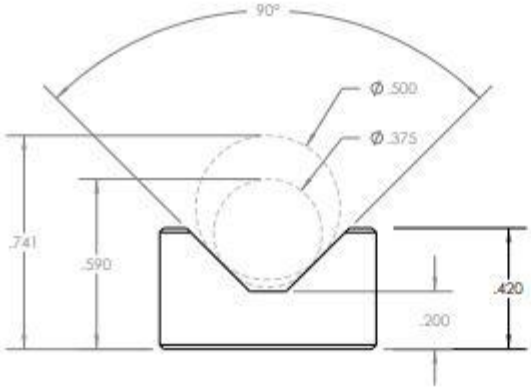

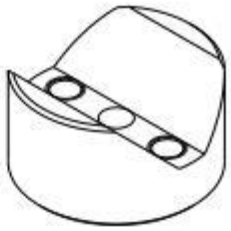

PROPRIETARY INFORMATION THE INFORMATION CONTAINED IN THIS DRAWING IS THE SOLE PROPERTY OF MICRO SURFACE ENGR. INC. AND IS FURNISHED FOR INFORMATIONAL PURPOSES ONLY. © 2006 MICRO SURFACE ENGR. INC.	UNLESS OTHERWISE SPECIFIED: DIMENSIONS ARE IN INCHES TOLERANCES: ANGULAR: ±° TWO PLACE DECIMAL ±.01 THREE PLACE DECIMAL ±.005 INTERPRET GEOMETRIC TOLERANCING PER: ANSI Y14.5	**Bal-tec** 1550 E. SLAUSON AVE LOS ANGELES, CA 90011				
		TITLE 3/8" VEE BLOCK - SURFACE MOUNT			NUMBER VB-375-SM	REV 001
		ENGINEER GENE GLEASON	DWN BY RJV	DATE DRAWN 6/4/07	SIZE A	SCALE 2:1	PAGE 1 OF 1

MATERIAL: STAINLESS STEEL 440C, HARDENED TO Rc 58 MIN

REV	ECO NO.	ECO TITLE	DATE
---	------	------	--/--/--

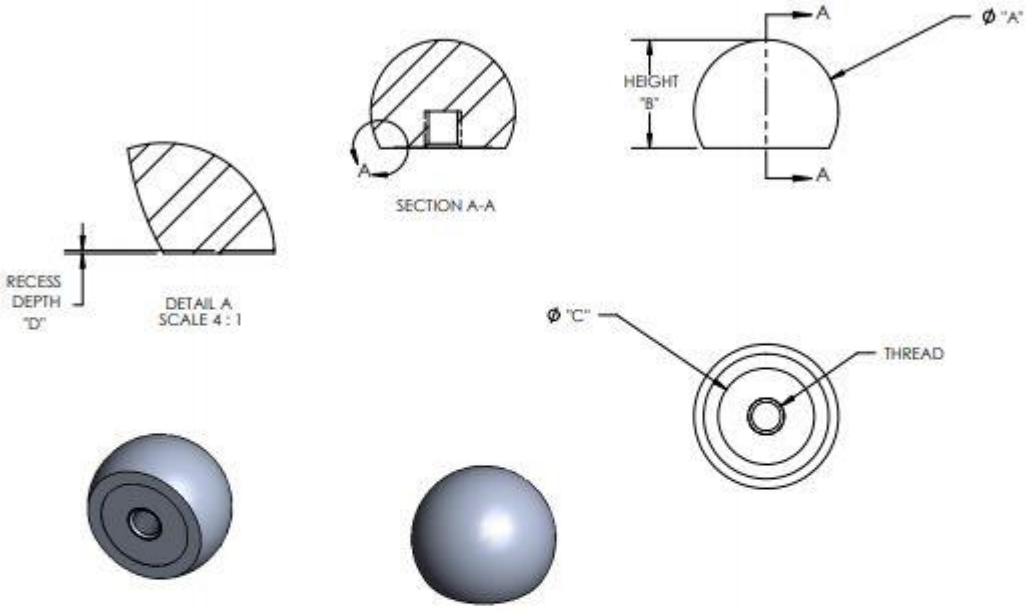

PART NUMBER	DIAMETER "A"	SHPERICITY	SURFACE ROUGHNESS MAX	HEIGHT "B"	RECESS DIA "C"	RECESS DEPTH "D"	THREAD	MIN THREAD DEPTH
250-TBR-T	0.250 ± .0001	0.000010	.7 Micro Inch Ra	0.167 ± .002	0.175	0.005	#4-40	0.094
312-TBR-T	0.3125 ± .0001	0.000010	.7 Micro Inch Ra	0.208 ± .002	0.200	0.005	#6-32	0.150
375-TBR-T	0.375 ± .0001	0.000010	.7 Micro Inch Ra	0.250 ± .002	0.250	0.005	#10-32	0.200
500-TBR-T	0.500 ± .0001	0.000010	.7 Micro Inch Ra	0.334 ± .002	0.325	0.005	1/4-20	0.250
750-TBR-T	0.750 ± .0001	0.000010	.7 Micro Inch Ra	0.500 ± .002	0.500	0.005	1/4-20	0.250
100-TBR-T	1.000 ± .0001	0.000010	.7 Micro Inch Ra	0.750 ± .002	0.666	0.005	1/4-20	0.250

UNLESS OTHERWISE SPECIFIED:

DIMENSIONS ARE IN INCHES

TOLERANCES:
ANGULAR: 1°
TWO PLACE DECIMAL ±.01
THREE PLACE DECIMAL ±.005

INTERPRET GEOMETRIC TOLERANCING PER: ANSI Y14.5

Bal-tec
1550 E. SLAUSON AVE
LOS ANGELES, CA 90011

TITLE	NUMBER	REV
TRUNCATED AND THREADED BALL	SEE TABLE	01

ENGINEER	DWN BY	DATE DRAWN	SIZE	SCALE	PAGE
GENE GLEASON	RJV	12/02/06	A	1:1	1 OF 1

APPENDIX B – REFERENCE POSITIONS OF THE SPHERES, MEASURED BY CMM, AND THEIR UNCERTAINTIES

Following table presents the measured reference positions of the spheres, the uncertainties of the measured position for each sphere in X, Y, and Z directions separately, and the total uncertainty of each sphere.

Sphere's no.	Location in X-Axis (mm)	Location in Y-Axis (mm)	Location in Z-Axis (mm)	Uncertainty of the measured location in X-direction (μm)	Uncertainty of the measured location in Y-direction (μm)	Uncertainty of the measured location in Z-direction (μm)	Total uncertainty
1	26.064	12.158	41.858	0.54	0.97	1.12	1.57
2	46.063	12.213	41.841	0.55	0.82	1.18	1.54
3	66.062	12.275	41.84	0.40	0.79	1.29	1.56
4	86.06	12.336	41.831	0.18	0.69	1.04	1.26
5	106.06	12.396	41.827	0.16	0.72	1.15	1.37
6	126.058	12.453	41.824	0.19	0.75	1.02	1.28
7	146.057	12.51	41.822	0.27	0.64	1.05	1.26
8	166.052	12.569	41.821	0.41	0.70	1.03	1.31
9	186.053	12.63	41.804	0.49	0.71	0.99	1.31
10	26.003	32.153	41.877	0.46	0.56	1.12	1.34
11	46.004	32.212	41.864	0.46	0.56	1.12	1.34
12	66	32.27	41.863	0.37	0.45	1.06	1.21
13	85.999	32.331	41.85	0.20	0.47	0.97	1.10
14	105.999	32.39	41.845	0.25	0.44	0.90	1.03
15	125.997	32.451	41.844	0.24	0.48	0.97	1.10
16	145.995	32.509	41.841	0.27	0.52	1.03	1.18

Sphere's no.	Location in X-Axis (mm)	Location in Y-Axis (mm)	Location in Z-Axis (mm)	Uncertainty of the measured location in X-direction (μm)	Uncertainty of the measured location in Y-direction (μm)	Uncertainty of the measured location in Z-direction (μm)	Total uncertainty
17	165.993	32.566	41.831	0.44	0.37	1.05	1.20
18	185.991	32.625	41.83	0.48	0.36	0.92	1.10
19	25.943	52.151	41.898	0.43	0.33	0.98	1.12
20	45.944	52.209	41.895	0.23	0.32	1.03	1.10
21	65.94	52.267	41.879	0.09	0.32	1.10	1.14
22	85.939	52.326	41.874	0.08	0.26	1.02	1.06
23	105.936	52.388	41.867	0.13	0.39	1.09	1.17
24	125.938	52.448	41.862	0.20	0.38	1.05	1.14
25	145.933	52.506	41.863	0.26	0.41	1.02	1.13
26	165.934	52.567	41.844	0.27	0.34	1.03	1.12
27	185.93	52.627	41.856	0.34	0.36	0.94	1.06
28	25.89	72.141	41.896	0.41	0.29	1.04	1.16
29	45.885	72.211	41.92	0.34	0.27	1.03	1.12
30	65.883	72.271	41.914	0.25	0.20	0.99	1.04
31	85.881	72.33	41.902	0.14	0.22	1.04	1.08
32	105.88	72.39	41.894	0.24	0.29	1.02	1.09
33	125.878	72.451	41.887	0.15	0.34	1.05	1.12
34	145.875	72.509	41.882	0.11	0.32	0.95	1.00
35	165.873	72.568	41.877	0.13	0.42	1.02	1.11
36	185.872	72.626	41.871	0.23	0.50	0.96	1.11
37	25.827	92.148	41.951	0.38	0.19	0.86	0.96

Sphere's no.	Location in X-Axis (mm)	Location in Y-Axis (mm)	Location in Z-Axis (mm)	Uncertainty of the measured location in X-direction (μm)	Uncertainty of the measured location in Y-direction (μm)	Uncertainty of the measured location in Z-direction (μm)	Total uncertainty
38	45.826	92.21	41.945	0.34	0.23	1.02	1.10
39	65.824	92.269	41.934	0.29	0.22	0.88	0.95
40	85.822	92.329	41.929	0.18	0.25	1.00	1.05
41	105.821	92.389	41.923	0.23	0.18	1.02	1.06
42	125.819	92.449	41.92	0.20	0.46	1.02	1.14
43	145.817	92.509	41.915	0.40	0.37	0.91	1.06
44	165.815	92.569	41.909	0.52	0.59	0.78	1.11
45	185.812	92.628	41.91	0.21	0.47	1.00	1.12
46	25.763	112.15	41.98	0.42	0.13	1.00	1.09
47	45.763	112.208	41.976	0.36	0.11	1.19	1.25
48	65.764	112.269	41.969	0.36	0.19	0.97	1.05
49	85.762	112.327	41.959	0.32	0.25	1.00	1.08
50	105.761	112.386	41.955	0.40	0.21	1.16	1.24
51	125.761	112.446	41.953	0.29	0.38	0.99	1.10
52	145.758	112.506	41.945	0.27	0.32	0.89	0.98
53	165.757	112.568	41.945	0.31	0.26	0.87	0.96
54	185.756	112.626	41.943	0.21	0.43	0.99	1.10
55	26.145	12.313	72.52	0.24	0.43	0.77	0.91
56	46.144	12.369	72.503	0.20	0.41	0.75	0.88
57	66.143	12.431	72.503	0.07	0.37	0.76	0.85
58	86.141	12.493	72.495	0.14	0.45	0.88	1.00

Sphere's no.	Location in X-Axis (mm)	Location in Y-Axis (mm)	Location in Z-Axis (mm)	Uncertainty of the measured location in X-direction (μm)	Uncertainty of the measured location in Y-direction (μm)	Uncertainty of the measured location in Z-direction (μm)	Total uncertainty
59	106.141	12.554	72.492	0.28	0.43	0.86	1.00
60	126.139	12.612	72.489	0.32	0.34	0.73	0.86
61	146.138	12.671	72.489	0.18	0.50	0.78	0.95
62	166.133	12.73	72.488	0.27	0.45	0.87	1.01
63	186.133	12.792	72.472	0.26	0.28	0.67	0.77
64	26.083	32.308	72.529	0.19	0.43	0.88	1.00
65	46.084	32.368	72.517	0.19	0.43	0.88	1.00
66	66.081	32.427	72.517	0.11	0.38	0.72	0.83
67	86.08	32.489	72.504	0.15	0.38	0.80	0.90
68	106.079	32.549	72.5	0.17	0.46	0.78	0.92
69	126.077	32.61	72.5	0.19	0.39	0.87	0.98
70	146.075	32.67	72.498	0.08	0.42	0.76	0.87
71	166.073	32.727	72.488	0.15	0.43	0.73	0.86
72	186.071	32.787	72.489	0.19	0.30	0.81	0.88
73	26.022	52.306	72.541	0.15	0.39	0.80	0.91
74	46.023	52.365	72.539	0.13	0.42	0.81	0.92
75	66.019	52.423	72.524	0.28	0.35	0.86	0.97
76	86.018	52.484	72.519	0.20	0.31	0.80	0.88
77	106.016	52.547	72.513	0.15	0.40	0.74	0.85
78	126.017	52.607	72.509	0.21	0.43	0.87	0.99
79	146.012	52.667	72.51	0.16	0.38	0.85	0.95

Sphere's no.	Location in X-Axis (mm)	Location in Y-Axis (mm)	Location in Z-Axis (mm)	Uncertainty of the measured location in X-direction (μm)	Uncertainty of the measured location in Y-direction (μm)	Uncertainty of the measured location in Z-direction (μm)	Total uncertainty
80	166.013	52.728	72.492	0.23	0.38	0.86	0.96
81	186.009	52.789	72.504	0.13	0.45	0.86	0.98
82	25.968	72.296	72.53	0.15	0.27	0.68	0.75
83	45.963	72.367	72.554	0.16	0.39	0.79	0.89
84	65.962	72.428	72.548	0.21	0.36	0.88	0.97
85	85.959	72.488	72.538	0.15	0.40	0.83	0.93
86	105.959	72.549	72.531	0.23	0.31	0.69	0.79
87	125.957	72.61	72.523	0.23	0.34	0.88	0.97
88	145.954	72.67	72.52	0.23	0.27	0.86	0.93
89	165.952	72.73	72.515	0.21	0.40	0.98	1.08
90	185.95	72.788	72.51	0.12	0.37	0.78	0.87
91	25.904	92.303	72.575	0.11	0.23	0.84	0.88
92	45.904	92.366	72.569	0.13	0.41	0.81	0.92
93	65.902	92.426	72.559	0.26	0.43	0.92	1.05
94	85.9	92.487	72.555	0.28	0.46	0.99	1.13
95	105.898	92.548	72.55	0.13	0.34	0.87	0.94
96	125.897	92.609	72.548	0.19	0.50	0.94	1.08
97	145.895	92.669	72.544	0.22	0.49	0.91	1.06
98	165.893	92.73	72.538	0.31	0.43	0.87	1.02
99	185.889	92.79	72.54	0.16	0.43	0.79	0.92
100	25.839	112.305	72.595	0.17	0.45	0.79	0.93

Sphere's no.	Location in X-Axis (mm)	Location in Y-Axis (mm)	Location in Z-Axis (mm)	Uncertainty of the measured location in X-direction (μm)	Uncertainty of the measured location in Y-direction (μm)	Uncertainty of the measured location in Z-direction (μm)	Total uncertainty
101	45.84	112.365	72.591	0.26	0.36	1.04	1.13
102	65.84	112.426	72.585	0.29	0.46	0.79	0.96
103	85.839	112.485	72.576	0.19	0.37	0.84	0.94
104	105.837	112.544	72.572	0.15	0.41	0.77	0.89
105	125.837	112.606	72.572	0.22	0.32	0.84	0.92
106	145.835	112.666	72.564	0.20	0.43	0.70	0.85
107	165.833	112.729	72.565	0.22	0.33	0.86	0.94
108	185.832	112.788	72.563	0.19	0.30	0.92	0.98
109	25.818	12.113	102.439	0.43	0.45	0.54	0.82
110	45.817	12.161	102.412	0.34	0.44	0.45	0.72
111	65.816	12.214	102.401	0.31	0.50	0.43	0.74
112	85.814	12.267	102.382	0.26	0.44	0.35	0.62
113	105.814	12.318	102.368	0.34	0.40	0.43	0.68
114	125.812	12.367	102.355	0.13	0.45	0.42	0.63
115	145.811	12.417	102.344	0.24	0.48	0.46	0.71
116	165.806	12.467	102.332	0.18	0.53	0.50	0.75
117	185.806	12.52	102.306	0.22	0.54	0.48	0.76
118	25.765	32.108	102.457	0.36	0.40	0.58	0.79
119	45.766	32.159	102.434	0.36	0.40	0.58	0.79
120	65.762	32.209	102.423	0.27	0.36	0.48	0.66
121	85.762	32.262	102.4	0.13	0.33	0.52	0.63

Sphere's no.	Location in X-Axis (mm)	Location in Y-Axis (mm)	Location in Z-Axis (mm)	Uncertainty of the measured location in X-direction (μm)	Uncertainty of the measured location in Y-direction (μm)	Uncertainty of the measured location in Z-direction (μm)	Total uncertainty
122	105.761	32.313	102.385	0.25	0.35	0.41	0.59
123	125.759	32.365	102.374	0.31	0.43	0.55	0.77
124	145.757	32.416	102.361	0.20	0.32	0.54	0.66
125	165.755	32.464	102.341	0.19	0.4	0.61	0.75
126	185.753	32.515	102.331	0.25	0.36	0.54	0.69
127	25.714	52.107	102.478	0.16	0.39	0.62	0.75
128	45.714	52.156	102.465	0.16	0.40	0.50	0.66
129	65.711	52.205	102.439	0.39	0.36	0.56	0.77
130	85.709	52.257	102.424	0.28	0.35	0.67	0.81
131	105.707	52.311	102.406	0.10	0.28	0.67	0.73
132	125.708	52.363	102.392	0.32	0.43	0.45	0.70
133	145.703	52.412	102.382	0.09	0.36	0.51	0.63
134	165.704	52.465	102.353	0.15	0.42	0.49	0.66
135	185.7	52.517	102.355	0.22	0.40	0.65	0.79
136	25.669	72.096	102.475	0.15	0.34	0.54	0.65
137	45.663	72.158	102.488	0.10	0.19	0.63	0.66
138	65.662	72.21	102.472	0.33	0.37	0.65	0.82
139	85.66	72.262	102.451	0.17	0.36	0.48	0.62
140	105.659	72.313	102.433	0.15	0.22	0.53	0.59
141	125.657	72.365	102.415	0.15	0.27	0.57	0.65
142	145.654	72.416	102.4	0.20	0.40	0.55	0.71

Sphere's no.	Location in X-Axis (mm)	Location in Y-Axis (mm)	Location in Z-Axis (mm)	Uncertainty of the measured location in X-direction (μm)	Uncertainty of the measured location in Y-direction (μm)	Uncertainty of the measured location in Z-direction (μm)	Total uncertainty
143	165.652	72.467	102.385	0.11	0.34	0.66	0.75
144	185.651	72.516	102.369	0.11	0.38	0.57	0.70
145	25.613	92.104	102.528	0.16	0.41	0.72	0.84
146	45.613	92.157	102.512	0.15	0.30	0.55	0.65
147	65.611	92.208	102.491	0.19	0.29	0.63	0.72
148	85.609	92.261	102.476	0.22	0.35	0.46	0.61
149	105.608	92.312	102.461	0.21	0.32	0.49	0.62
150	125.606	92.364	102.448	0.09	0.37	0.54	0.67
151	145.604	92.415	102.433	0.20	0.32	0.51	0.63
152	165.602	92.467	102.417	0.24	0.30	0.59	0.70
153	185.599	92.518	102.408	0.21	0.41	0.58	0.74
154	25.558	112.105	102.557	0.19	0.33	0.63	0.74
155	45.558	112.156	102.543	0.18	0.33	0.64	0.74
156	65.559	112.208	102.526	0.15	0.29	0.48	0.58
157	85.557	112.258	102.506	0.26	0.29	0.64	0.75
158	105.556	112.309	102.491	0.27	0.37	0.54	0.71
159	125.555	112.361	102.48	0.26	0.43	0.50	0.71
160	145.553	112.412	102.462	0.05	0.41	0.74	0.84
161	165.551	112.466	102.451	0.23	0.38	0.55	0.71
162	185.551	112.516	102.439	0.22	0.31	0.64	0.74
163	25.894	12.297	133.1	2.52	1.74	1.04	3.24

Sphere's no.	Location in X-Axis (mm)	Location in Y-Axis (mm)	Location in Z-Axis (mm)	Uncertainty of the measured location in X-direction (μm)	Uncertainty of the measured location in Y-direction (μm)	Uncertainty of the measured location in Z-direction (μm)	Total uncertainty
164	45.893	12.345	133.074	2.49	1.73	1.14	3.24
165	65.892	12.398	133.064	2.15	1.81	1.29	3.09
166	85.89	12.452	133.046	1.79	1.73	1.29	2.81
167	105.89	12.504	133.032	1.70	1.67	1.28	2.70
168	125.888	12.553	133.02	1.41	1.72	1.25	2.55
169	145.887	12.603	133.009	1.12	1.73	1.35	2.47
170	165.882	12.654	132.998	0.84	1.65	1.42	2.33
171	185.882	12.707	132.972	0.72	1.63	1.36	2.24
172	25.841	32.292	133.109	2.51	1.78	1.28	3.33
173	45.842	32.343	133.087	2.51	1.78	1.28	3.33
174	65.838	32.394	133.076	1.86	2.01	1.26	3.01
175	85.837	32.447	133.054	1.62	1.84	1.25	2.75
176	105.836	32.498	133.039	1.22	1.84	1.31	2.57
177	125.835	32.551	133.03	1.20	1.72	1.40	2.53
178	145.833	32.601	133.017	1.04	1.67	1.41	2.42
179	165.831	32.65	132.998	0.63	1.74	1.48	2.37
180	185.829	32.702	132.988	0.36	1.82	1.32	2.28
181	25.789	52.291	133.12	2.43	1.93	1.23	3.33
182	45.789	52.341	133.108	2.11	1.84	1.32	3.09
183	65.786	52.39	133.083	1.74	2.05	1.42	3.04
184	85.784	52.442	133.068	2.11	2.15	1.61	3.42

Sphere's no.	Location in X-Axis (mm)	Location in Y-Axis (mm)	Location in Z-Axis (mm)	Uncertainty of the measured location in X-direction (μm)	Uncertainty of the measured location in Y-direction (μm)	Uncertainty of the measured location in Z-direction (μm)	Total uncertainty
185	105.782	52.496	133.051	1.32	1.90	1.27	2.64
186	125.783	52.548	133.037	1.06	2.07	1.37	2.70
187	145.778	52.599	133.029	0.79	1.83	1.43	2.45
188	165.779	52.651	133	0.55	2.04	1.32	2.49
189	185.775	52.703	133.003	0.37	1.91	1.38	2.38
190	25.744	72.28	133.108	2.75	2.12	1.44	3.76
191	45.738	72.343	133.122	2.04	2.19	1.26	3.24
192	65.737	72.395	133.107	1.80	2.08	1.23	3.02
193	85.735	72.446	133.086	1.51	2.02	1.43	2.90
194	105.734	72.498	133.069	1.09	2.17	1.33	2.77
195	125.732	72.551	133.051	0.83	2.08	1.49	2.69
196	145.729	72.602	133.037	0.57	2.18	1.56	2.74
197	165.727	72.653	133.023	0.38	2.07	1.41	2.53
198	185.726	72.703	133.008	0.29	1.97	1.47	2.48
199	25.688	92.288	133.152	2.08	2.32	1.41	3.42
200	45.688	92.341	133.137	1.91	2.29	1.46	3.32
201	65.686	92.393	133.116	1.75	2.25	1.3	3.14
202	85.684	92.446	133.102	1.44	2.26	1.37	3.01
203	105.682	92.497	133.087	1.10	2.30	1.48	2.95
204	125.681	92.55	133.075	0.87	2.21	1.52	2.82
205	145.679	92.601	133.061	0.58	2.24	1.47	2.74

Sphere's no.	Location in X-Axis (mm)	Location in Y-Axis (mm)	Location in Z-Axis (mm)	Uncertainty of the measured location in X-direction (μm)	Uncertainty of the measured location in Y-direction (μm)	Uncertainty of the measured location in Z-direction (μm)	Total uncertainty
206	165.677	92.654	133.045	0.30	2.28	1.62	2.81
207	185.674	92.705	133.037	0.34	2.18	1.53	2.68
208	25.632	112.289	133.171	2.13	2.60	1.47	3.67
209	45.633	112.341	133.158	1.84	2.65	1.64	3.62
210	65.633	112.393	133.141	1.61	2.65	1.60	3.49
211	85.632	112.443	133.122	1.38	2.55	1.51	3.27
212	105.63	112.494	133.108	1.02	2.21	1.31	2.77
213	125.63	112.547	133.098	0.80	2.56	1.63	3.14
214	145.627	112.598	133.08	0.52	2.57	1.50	3.02
215	165.626	112.652	133.071	0.43	2.43	1.59	2.94
216	185.625	112.702	133.059	0.47	2.48	1.42	2.90

APPENDIX C – TABLE OF DIFFERENT NOMINAL MEASURED LENGTHS AND NUMBER OF THE MEASUREMENTS

Length's number	Nominal measured lengths	Number of measurements
1	20	372
2	28.2843	320
3	31	162
4	36.8917	558
5	40	312
6	41.9643	480
7	44.7214	536
8	50.6063	468
9	54.4151	804
10	56.5685	224
11	60	252
12	62	108
13	63.2456	432
14	64.5058	336
15	65.1460	372
16	67.5352	378
17	68.1469	320
18	70.4344	648

Length's number	Nominal measured lengths	Number of measurements
19	72.1110	360
20	73.7835	312
21	76.4461	536
22	78.4920	540
23	80	192
24	82.4621	328
25	83.9285	224
26	84.8528	144
27	85.7963	288
28	86.2786	252
29	88.0965	492
30	88.5664	432
31	89.4427	272
32	90.3383	216
33	93	54
34	94.6626	408
35	95.0999	360
36	95.1262	186

Length's number	Nominal measured lengths	Number of measurements
37	97.2060	160
38	100	348
39	101.2126	192
40	101.2373	156
41	101.9804	224
42	103.1698	328
43	103.1940	268
44	104.6948	522
45	105.0904	144
46	106.5880	336
47	107.7033	184
48	108.8301	272
49	108.8531	112
50	110.6752	126
51	112.0759	276
52	112.4678	216
53	113.1371	80
54	116.6190	144
55	117.3073	120
56	117.6605	348
57	117.6818	180
58	119.3482	224

Length's number	Nominal measured lengths	Number of measurements
59	120	72
60	120.6690	216
61	121.6553	120
62	122.6744	96
63	123.9395	108
64	124.2739	184
65	124.2940	164
66	125.5428	180
67	125.8928	72
68	126.4911	96
69	128.0625	104
70	129.0116	80
71	129.0310	136
72	130.2344	144
73	131.7611	156
74	132.0757	144
75	134.1641	72
76	135.0704	72
77	136.5430	120
78	136.5613	174
79	137.6989	108
80	138.0181	112

Length's number	Nominal measured lengths	Number of measurements
81	140	48
82	140.8687	96
83	141.4214	112
84	142.2814	104
85	142.2990	92
86	143.3911	72
87	144.2221	48
88	144.7791	168
89	145.6022	64
90	146.4548	40
91	147.5161	72
92	147.7972	72
93	148.8657	96
94	149.1610	72
95	151.8190	36
96	152.3155	48
97	153.1143	48
98	153.1307	60
99	154.4150	112
100	155.4381	72
101	156.2050	24
102	156.9841	48

Length's number	Nominal measured lengths	Number of measurements
103	157	48
104	158.2530	64
105	158.2688	52
106	159.2514	36
107	160	24
108	161.2452	72
109	162.9755	36
110	163.2452	36
111	164.1981	108
112	164.4506	48
113	164.9242	32
114	167.8124	48
115	168.0595	24
116	168.0744	24
117	169.2602	56
118	170.8801	24
119	171.5925	24
120	171.6071	24
121	172.0465	16
122	172.7542	72
123	172.7686	32
124	173.6692	36

Length's number	Nominal measured lengths	Number of measurements
125	174.8170	24
126	176.1931	32
127	178.4629	24
128	178.8854	16
129	181.5516	24
130	181.7801	24
131	181.7938	12
132	182.8770	16
133	185.0649	12
134	186.1424	36

Length's number	Nominal measured lengths	Number of measurements
135	188.6796	8
136	189.3251	16
137	189.3383	16
138	191.2093	12
139	194.5482	12
140	195.5735	8
141	198.6051	8
142	201.6160	8
143	210.3545	4

APPENDIX D – DESIGNED CALIBRATION AND PERFORMANCE EVALUATION ARTIFACTS IN THE PREVIOUS WORKS IN THIS AREA

The designed artifacts to calibrate or evaluate the performance of 3D scanners are presented in the following figures. These figures are classified by the their publication year.

Designed artifact by Qiang et al. 2009 [20]

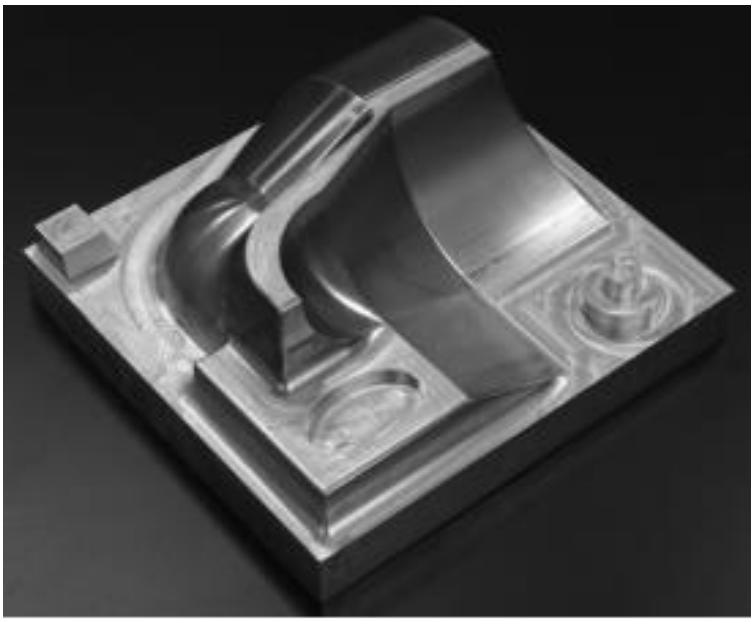

Designed artifact by Iuliano et al. 2010 [13]

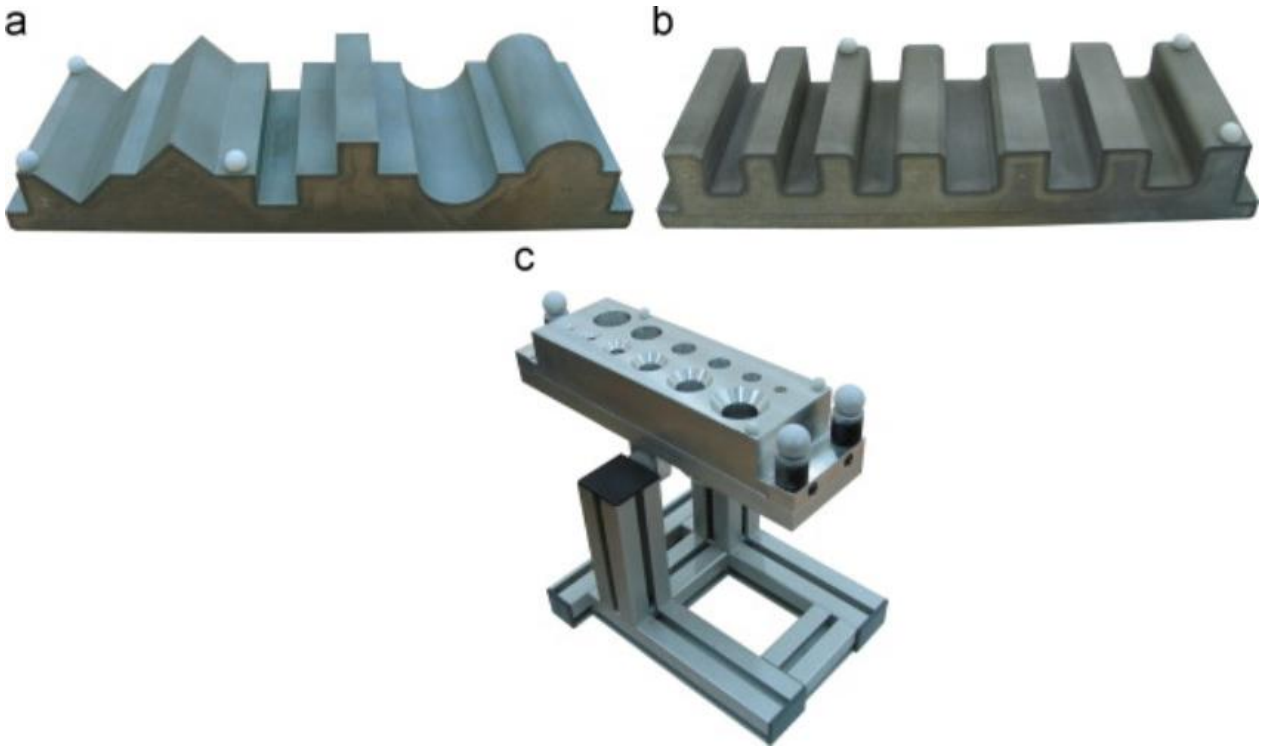

Designed artifact by Martínez et al. 2010 [22]

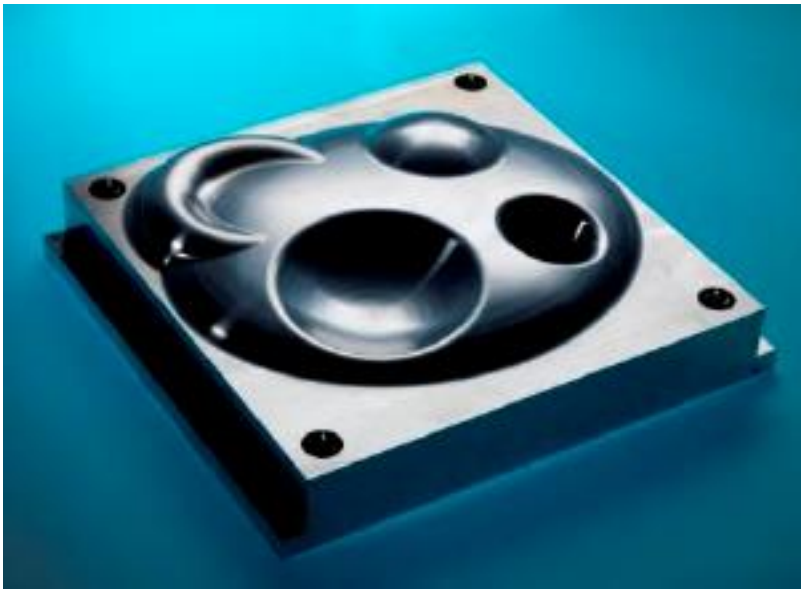

Designed artifact by McCarthy et al. 2011 [15]

(a) (b)

Designed artifacts by Acko et al. 2012 [17]

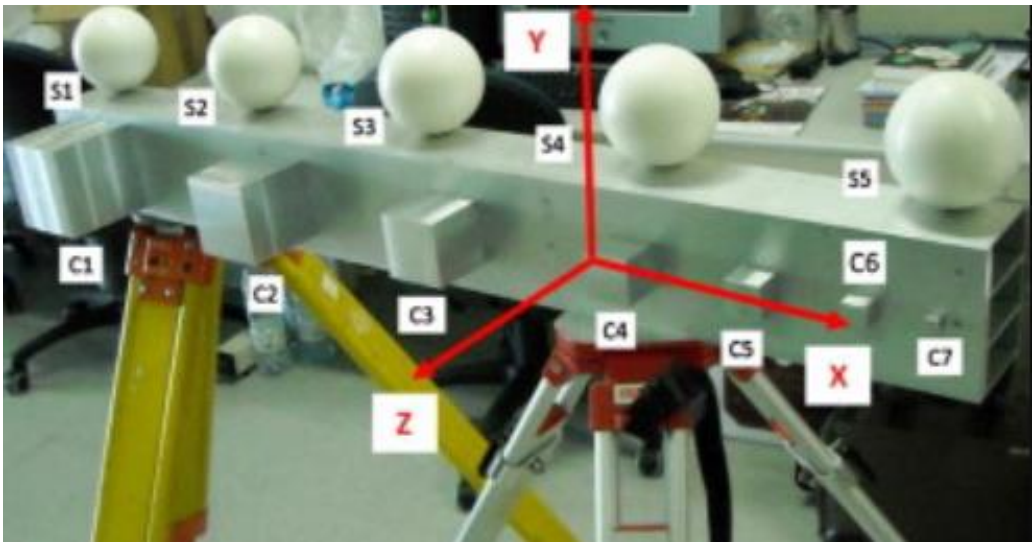

Designed artifact by Gonzalez-Jorge et al. 2013 [23]

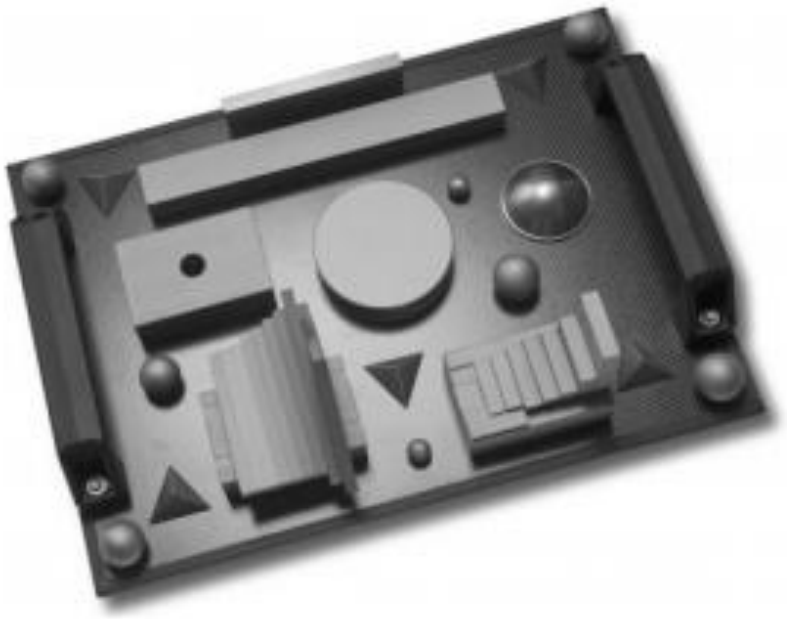

Designed artifact by MacKinnon et al. 2013 [14]

Designed artifact by Genta et al. 2016 [21]

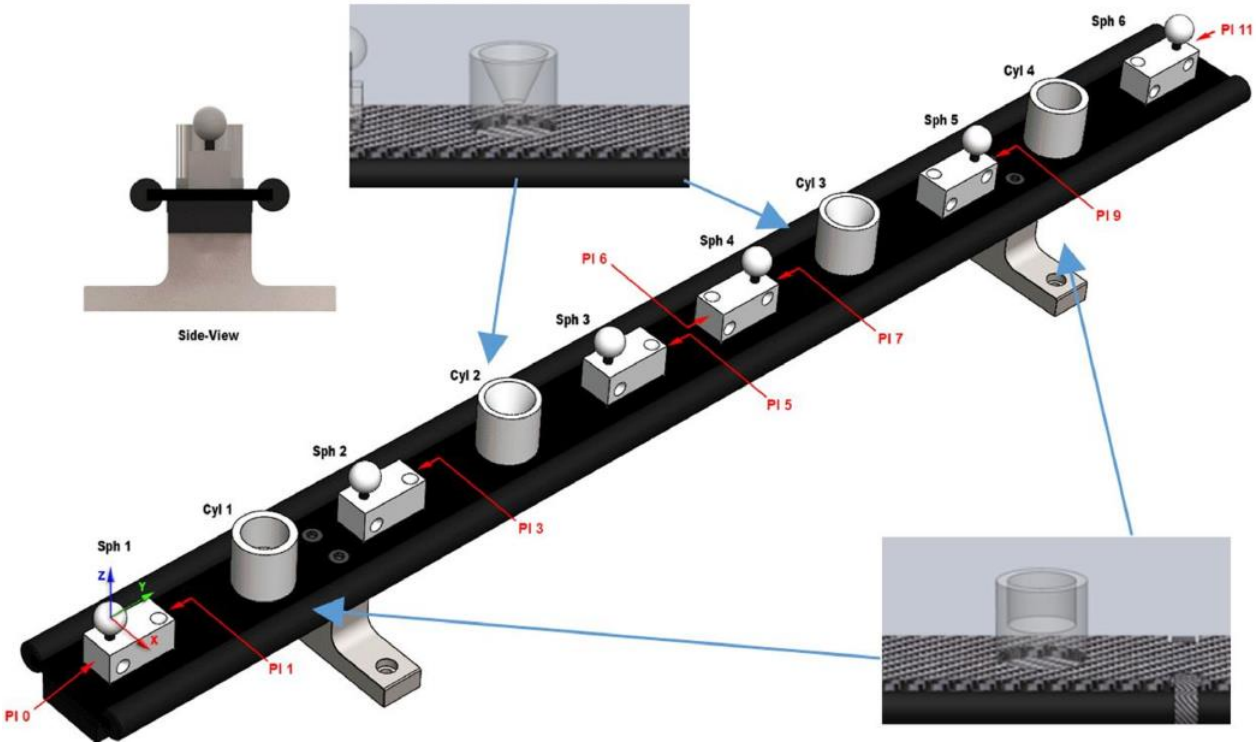

Designed artifact by Martínez-Pellitero et al. 2018 [18]